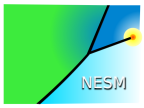

Bachelor's Thesis

Erzeugung eines homogenen, stationären Zustandes eines granularen Gases aus einem inhomogenen Zustand

The generation of a homogeneous, steady state in granular gases from an inhomogeneous state

prepared by

Marius Herr

from Fulda

at the Max Planck Institute for Dynamics and Self-Organization

Thesis period:	8th July 2015 until 15th October 2015
Supervisor:	Dr. Marco G. Mazza
First Rreferee:	Dr. Marco G. Mazza
Second referee:	Prof. Dr. Annette Zippelius

Contents

1 Introduction **1**

2 Overview **3**

3 Theoretical Description **5**

3.1 Granular gases 5
3.2 Hydrodynamic description 6
3.3 Equation of state 8
3.4 Conservative form of the hydrodynamic equations 9
3.5 Haff's law 10
3.6 Critical system size 12
3.7 The homogeneous, steady state 13

4 Numerical and technical details **15**

5 Preparations **17**

5.1 General system parameter 17
5.2 Freely cooling granular gases 17
5.3 Description of the shaking process 19
5.3.1 Introduction 19
5.3.2 Shifting the reference frame 20
5.3.3 Choice of the initial phase 21
5.3.4 Measuring the oscillation of a Gaussian density distribution . 22
5.3.5 Transient and decay procedure 22
5.4 Critical system size 25
5.5 The initial state 27

6 Results **31**

6.1 Shaking perpendicular to the density gradient 31

6.2 Shaking parallel to the density gradient 34

6.2.1 Varying f and A 39

6.3 All-sided vibration 40

7 Summary and discussion **47**

1 Introduction

This Bachelor thesis deals with computer simulations of a granular gas. A granular gas consists of macroscopic particles which collide inelastically [1]. Due to the loss of kinetic energy through collisions, the thermal energy inside the colliding particles increases. This behavior contrasts with molecular gases, where exclusively elastic collisions occur. Examples of a granular gas are sprayed sand, cosmic clouds of dust and planetary rings [2].

To analyze and understand the behavior of granular gases, a variety of experiments are necessary. It is particular helpful to perform these experiments on ground instead of observing granular gases with telescopes and space probes, so that specific parameters and properties of the gas could be tuned by the experimenter.

A characteristic phenomenon of granular gases, is the self-organized formation of density patterns out of a homogeneous distribution. These pattern formation was shown in many investigations based on computer simulations [3].
In order to measure such patterns in experiments and to determine its cooling characteristics, microgravity experiments in suborbital rockets are performed. For this cuboid containers are used which include the granular material [4].
The ideal starting point of these experiments is a homogeneous density distribution. But, because gravity and other pertubations generate sedimentation or other inhomogeneities before the experiments start, these dense regions have to be dissolved.

Attempting to dissolve density inhomogeneities is exactly the aim of the thesis. With the aid of computer simulations, which solve the hydrodynamic equations for granular gases, an inhomogeneous density field should be homogenized to create a starting condition for the experiments. The homogenization is made through a vibration of the container walls, that is, through an external energy supply. We discuss different protocols used, and whether they succeed or not.

2 Overview

Chapter (3) gives an overview over the theoretical base and algorithms which will be used during the thesis:
The assumptions that are chosen to describe the model of a granular gas and further explanations are listed in Chap. (3.1). Sections (3.2)-(3.4) describe the hydrodynamic theory of a granular gas. In Sec. (3.5), the cooling evolution in a force free environment is derived. The theoretical part ends with a explanation of a stability criterion and the explanation of a homogenous, steady state.
Chapter (4) gives the details of the numerical implementation.
The expedient steps to generate a homogenous state out of an inhomogeneous system without gravity begin in Sec. (5.3) with the development of a certain functional form of the wall-oscillation. In Sec. (6.1)-(6.3) we describe the impact of several parameters such as shaking frequency, amplitude, packing fraction, system size and parameters related to the protocol of the shaking. We explain appropriate parameters for the simulations and specify which set of parameter gives the best homogenous state. The last result in Sec. (6.3) shows a certain technique which is able to dissolve an arbitrary initial state.
This thesis ends with a summary and discussion of the obtained results.

3 Theoretical Description

3.1 Granular gases

In this section we give a detailed description of a granular gas. We follow the description in Ref. [1]. The starting point of the microscopic description is the pairwise collisions of macroscopic particles. One assume the occurrence of solely pairwise interactions in order to simplify the model. This assumption is justifiable if the mean free-flight time τ_f is much larger than the typical time of a collision τ_{coll}. In addition, it is assumed that even in denser regions, that is for a decreasing τ_f, the fraction $\tau_{\text{coll}}/\tau_f$ is vanishing. These condition is fulfilled for particles with insignificant elasticity and one therefore calls this approximation *hard-particle approximation*. Another simplification in this treatment is to consider identical particle radii and spherical (circular) particle shapes in 3D (2D) before and after a collision. During pairwise collisions the particles are temporally deformed and kinetic energy is transformed into internal degrees of freedom of the particles. For example, due to the lattice structure of the atoms inside the particles the kinetic energy turns into phonons. Nevertheless the average particle temperature increase ΔT_P per collision, merely is in the range of $10^{-3}K$.
The loss of energy can be expressed through the rate of the relative velocities before and after a collision

$$\varepsilon \equiv \frac{|v_1' - v_2'|}{|v_1 - v_2|} \equiv \frac{|v_{12}'|}{|v_{12}|}, \tag{3.1}$$

where v_i (v_i') is the velocity of particle i before (after) a collision and ε is called the coefficient of restitution. Due to the energy loss ε takes on values between 0 and 1.

If we assume a viscoelastic model for the particles, ε will depend on the tangential and normal velocity, particle masses, viscous constants, elastic constant, the Young modulus, and the Poisson ratio. Because of the essential simplifications of the math-

ematics and algorithms describing a granular gas, a constant ε is used in the thesis. The validity of this simplification, that is an ε which is independent of the above quantities, is established in Sec. (3.7). Thus, there are only three material parameters describing the particles: ε, the particle diameter σ and its mass m.

3.2 Hydrodynamic description

Alternative to the description of a granular fluid as composed of discrete particles, one can also adopt a macroscopic approach by defining the density, temperature, and velocity fields. The origin of the hydrodynamic approach is the microscopic kinetic theory based on pairwise particle collisions.
First of all, to express the hydrodynamic equations describing a granular gas, one need to introduce the velocity distribution function $f(\vec{r}, \vec{v}, t)$ where $\vec{v}$ is the velocity, $\vec{r}$ the position, and t the time. It is defined such that

$$f(\vec{r}, \vec{v}, t)\ \mathrm{d}^3\vec{r}\ \mathrm{d}^3\vec{v} \tag{3.2}$$

yields the number of particles inside the infinitesimal phase space volume $\mathrm{d}^3\vec{r}\ \mathrm{d}^3\vec{v}$ at the point $(\vec{r}, \vec{v})$ in phase space.
Due to this definition an integration over the whole phase space of a physical system gives the total number of particles N inside this system.

$$\int \mathrm{d}^3\vec{r} \int \mathrm{d}^3\vec{v} f(\vec{r}, \vec{v}, t) = N \tag{3.3}$$

One uses $f(\vec{r}, \vec{v}, t)$ to define the following macroscopic fields: number density $n(\vec{r}, t)$, average convective velocity $\vec{u}(\vec{r}, t)$ and granular temperature $T(\vec{r}, t)$.

$$n(\vec{r}, t) = \int \mathrm{d}^3v f(\vec{r}, \vec{v}, t) \tag{3.4}$$

$$n(\vec{r}, t)\vec{u}(\vec{r}, t) = \int \mathrm{d}^3v \vec{v} f(\vec{r}, \vec{v}, t) \tag{3.5}$$

$$\frac{f}{2} n(\vec{r}, t) T(\vec{r}, t) = \int \mathrm{d}^3v \frac{m\left(\vec{v} - \vec{u}(\vec{r}, t)\right)^2}{2} f(\vec{r}, \vec{v}, t), \qquad T = k_B \bar{T}\ . \tag{3.6}$$

T is in units of energy, that is it includes the Boltzmann constant. As it can be seen in Eq. (3.6) the granular temperature is proportional to the variance of the velocity. In the following we describe the hydrodynamic equations for a granular gas in two dimensions. These equations are derived from a corresponding Boltzmann transport equation. The Boltzmann equation is the fundamental equation of kinetic gas theory and combines the microscopic and macroscopic description of a gas. These derivations can be found in [1].
In contrast to the equations in [1], which describe a force free granular gas, the more general case with an external acceleration $\vec{a}(t)$ is presented.
The equations for the conservation of mass, momentum and energy are

$$\frac{\partial n}{\partial t} + \vec{\nabla} \cdot (n\vec{u}) = 0 \tag{3.7}$$

$$\frac{\partial \vec{u}}{\partial t} + \vec{u} \cdot \vec{\nabla}\vec{u} + (nm)^{-1}\vec{\nabla} \cdot \hat{P} - \vec{a}(t) = 0 \quad \text{with} \quad \vec{u} = \begin{pmatrix} u_x \\ u_y \end{pmatrix} \tag{3.8}$$

$$\frac{\partial T}{\partial t} + \vec{u} \cdot \vec{\nabla}T + \frac{1}{n}\left((\hat{P} : \vec{\nabla}\vec{u}) + \vec{\nabla} \cdot \vec{q}\right) + \zeta T = 0 \tag{3.9}$$

where $\hat{P}$ and $\vec{q}$ are the pressure tensor and heat flux, respectively

$$P_{ij} = p\delta_{ij} - \eta\left(\nabla_i u_j + \nabla_j u_i - \frac{2}{3}\delta_{ij}\vec{\nabla} \cdot \vec{u}\right) \tag{3.10}$$

$$\vec{q} = -\kappa\vec{\nabla}T - \mu\vec{\nabla}n \tag{3.11}$$

$$p = nT\left[1 + (1+\varepsilon)g(\sigma)\nu\right]. \tag{3.12}$$

p is the hydrostatic pressure, $\nu = 4n/(\pi\sigma^2)$ the packing fraction in two dimensions and $g(\sigma)$ the pair correlation function (see Chap. (3.3)).
The *energy equation* (3.9) describes the temporal evolution of the granular temperature. In contrast to the other equations and to molecular gases the total temperature of an isolated system is not a conserved quantity.

In the case of a constant coefficient of restitution ε the cooling rate ζ, the shear viscosity η, the coefficient μ and the thermal conductivity κ are a function of several

other quantities:

$$\zeta = \zeta(n, T, m, \varepsilon, \sigma), \qquad \mu = \mu(n, T, m, \varepsilon, \sigma), \tag{3.13}$$

$$\eta = \eta(T, m, \varepsilon, \sigma), \qquad \kappa = \kappa(T, m, \varepsilon, \sigma). \tag{3.14}$$

An exact derivation of these coefficients can be found in [1]. One should mention that the coefficient μ does not exist in the conventional hydrodynamics which only deals with elastic collisions. This coefficient μ appears in the term $\mu\vec{\nabla}n$ in the heat flux. By considering a granular gas one has to keep in mind that due to inelastic collisions, regions with higher densities n and therefore higher collision rates lose energy more quickly than regions with lower densities. Because of this it has an influence on the heat flux [5]. The term proportional to the density gradient is in principle present also for molecular fluids but the Onsager theorem protects against it yielding $\mu = 0$ [6].

3.3 Equation of state

In this section we describe further details of the equation of state (3.12). We follow Ref. [7]. Through the following rearrangement of the equation of state, a new dimensionless pressure P is defined, which solely depends on the packing fraction.

$$P \equiv \frac{p}{p_0} - 1 = \frac{p}{nT} - 1 = (1 + \varepsilon)g(\nu) \tag{3.15}$$

A measurement of the dependence on ν can be seen in Fig. (3.1). It shows the solid-liquid phase transition in a 2D simulation of a hard sphere gas occurring at a critical packing fraction $v_c \approx 0.7$. The reason of this transition is due to ordering effects close to ν_c which leads to an increased average free path-length and therefore to a decreasing pressure and collision rate.

To derive an equation of state which is valid for the whole density range, an appropriate functional form has to be found. The following functional form of the pair-correlation-function is a composition of theoretical predictions for certain density ranges and results from nonlinear regressions. It is arranged so that it fits the measured data in Fig. (3.1) as closely as possible. g_{Q} is finally the form that is used

in the performed simulations.

$$g_{\mathrm{Q}} = g_4 + m(\nu)[g_{\mathrm{dense}} - g_4], \tag{3.16}$$

$$g_4 = \frac{1 - 7\nu/16}{(1-\nu)^2} - \frac{\nu^3/6}{8(1-\nu)^4}, \tag{3.17}$$

$$m(\nu) = [1 + \exp(-(\nu - \nu_{\mathrm{c}})/m_v]^{-1}, \tag{3.18}$$

$$g_{\mathrm{dense}} = \frac{1}{\nu_m - \nu} h(\nu_m - \nu) - 1, \tag{3.19}$$

$$h(x) = 1 + c_1 x + c_3 x^3, \quad \text{with fit parameters} \quad c_1, c_3 \text{ and } m_v \tag{3.20}$$

where $\nu_m = \pi/(2\sqrt{3})$ represents the maximum packing fraction in two dimensions.

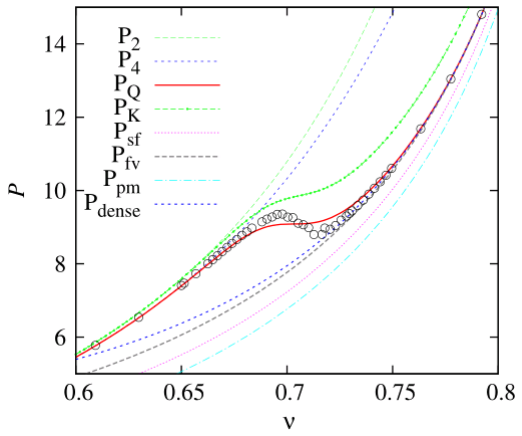

Figure 3.1: The dimensionless pressure P in dependence of the packing fraction ν is shown. The circles represent the measured data and the red curve displays P_Q, the best approximation [7].

3.4 Conservative form of the hydrodynamic equations

In order to prepare the hydrodynamic equations for the finite volume method, which is presented in Sec. (4), it is necessary to rewrite the equations in conservative form

$$\frac{\partial}{\partial t} w(\vec{r}, t) = -\vec{\nabla} \cdot f(w(\vec{r}, t)) + g(w(\vec{r}, t)), \tag{3.21}$$

where $w(\vec{r},t)$ is a hydrodynamical field, $f(w(\vec{r},t))$ is its associated flux, and $g(w(\vec{r},t))$ is a source term. If the source term $g(w(\vec{r},t))$ is zero, then $w(\vec{r},t)$ is a conserved physical quantity [8]. In the case of a force free molecular gas these quantities are the total energy

$$\rho E = \rho E_0(\vec{u}^2 + 2T/m), \tag{3.22}$$

$\rho\vec{u}$ and ρ, where ρ is the mass density [9]. The hydrodynamic equations of a granular gas expressed in conservative form are:

$$\frac{\partial n}{\partial t} = -\vec{\nabla}\cdot(n\vec{u}), \tag{3.23}$$

$$\begin{aligned}\frac{\partial}{\partial t}(\rho\vec{u}) &= \frac{\partial}{\partial t}(\rho)\vec{u} + \rho\frac{\partial}{\partial t}(\vec{u}) \\ &= -\left(m\vec{\nabla}\cdot(n\vec{u})\right)\vec{u} - \rho\left(\vec{u}\cdot\vec{\nabla}\vec{u} + (nm)^{-1}\vec{\nabla}\cdot\hat{P} - \vec{a}(t)\right) \\ &= -\vec{\nabla}\cdot\left(\rho\vec{u}\vec{u} + \hat{P}\right) + \rho\vec{a}(t),\end{aligned} \tag{3.24}$$

$$\begin{aligned}\frac{\partial}{\partial t}(\rho\cdot E) &= \frac{\partial}{\partial t}(\rho)\cdot E_0(\vec{u}^2 + 2T/m) + \rho E_0 2\vec{u}\cdot\frac{\partial}{\partial t}\vec{u} + 2nE_0\frac{\partial}{\partial t}T \\ &= -\left(\vec{\nabla}\cdot(\rho\vec{u})\right)\cdot E_0(\vec{u}^2 + 2T/m) + \rho E_0 2\vec{u}\cdot\left(\vec{u}\cdot\vec{\nabla}\vec{u} + (nm)^{-1}\vec{\nabla}\cdot\hat{P} - \vec{a}(t)\right) \\ &\quad - 2nE_0\left(\vec{u}\cdot\vec{\nabla}T + \frac{1}{n}\left((\hat{P}:\vec{\nabla}\vec{u}) + \vec{\nabla}\cdot\vec{q}\right) + \zeta T\right) \\ &= \vec{\nabla}\cdot\left(\vec{u}^2\rho\vec{u} + 2(\rho\vec{u}T) + 2(\hat{P}\cdot\vec{u}) + 2\vec{q}\right)E_0 + 2E_0(\zeta nT - \rho\vec{u}\cdot\vec{a}(t)).\end{aligned} \tag{3.25}$$

3.5 Haff's law

Because a granular gas loses thermal energy over time (see Eq. (3.9)), one is interested in the time dependent change of the granular temperature (Eq. (3.6)). We follow the derivation in [1] which refers to a homogeneous, isotropic, force-free and infinitely extended granular gas. It is valid during the transient state where the gas density remains homogeneous which is known as "homogeneous cooling state".

According to the model of a granular gas, the temperature decay ΔT during the interval Δt is proportional to the average energy loss $\langle\Delta E_{\mathrm{Kin}}\rangle$ per collision and to the number of collisions $\mu(\Delta t)$ per interval Δt. With the aid of Eq. (3.1) one is able

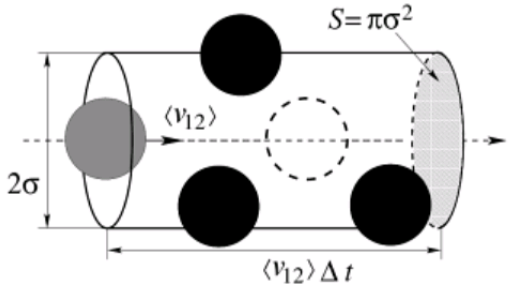

Figure 3.2: Schematic depiction of the collision cylinder [1].

to express the change of relative velocities before and after the collision $v'_{12} = \varepsilon v_{12}$.

$$\Delta T \propto \langle \Delta E_{\mathrm{Kin}} \rangle \, \mu(\Delta t) \tag{3.26}$$

$$\langle \Delta E_{\mathrm{Kin}} \rangle = \frac{m^{\mathrm{eff}}}{2} \left\langle {v'_{12}}^2 - {v_{12}}^2 \right\rangle = -\frac{m^{\mathrm{eff}}}{2} \left\langle {v_{12}}^2 \right\rangle (1-\varepsilon^2) \propto -(1-\varepsilon^2)T \tag{3.27}$$

One is allowed to replace the average kinetic energy $\langle {v_{12}}^2 \rangle$ with cT because of the absence of local flows, that is $\langle v \rangle^2 = 0$. To determine the number of collisions per interval $\mu(\Delta t)$ one assumes that a single particle i with diameter σ moves with the average relative velocity $\langle v_{12} \rangle$ whereas the other particles stay fixed. Because of that, $\mu(\Delta t)$ depends on the particle density n and on the size of the collision cylinder ΔV, which is the volume where particle i can collide with another particle during the time Δt (see Fig. (3.2)). A collision occurs if the geometric center of another particle is inside ΔV. The length of the cylinder is $\langle v_{12} \rangle \, \Delta t$.

$$\mu(\Delta t) = \Delta V n = \pi \sigma^2 \langle v_{12} \rangle \, \Delta t n \quad \propto \quad \sigma^2 \sqrt{T} \Delta t \tag{3.28}$$

By means of Eq. (3.26), (3.27) and (3.28) one can find an expression for the temperature decay rate

$$\frac{\mathrm{d}T}{\mathrm{d}t} \approx \frac{\Delta T}{\Delta t} \propto \frac{-(1-\varepsilon^2) T \sigma^2 \sqrt{T} \Delta t}{\Delta t} \tag{3.29}$$

By solving this differential equation with the initial condition $T(0) = T_0$ one finally finds Haff's law

$$T(t) = \frac{T_0}{(1 + t/\tau_0)^2} \quad \text{with} \quad \tau_0 \propto 1/(n\sigma^2(1-\varepsilon^2)\sqrt{T_0}) \tag{3.30}$$

3.6 Critical system size

In Fig. (5.1) the evolution of an initially homogenous, flux-free system can be seen. The development of density heterogeneities shows the instability of the initial state for the chosen parameters. One has to analyze the stability of the hydrodynamic equations in order to find criteria for cluster formation or instability of such an initial state. The extensive derivations of such criteria can be found in [1]. A short description of the essential steps follows below.

To study in first approximation the nonlinear, partial differential equations of granular hydrodynamics they have to be linearized. Otherwise it is not possible to find analytical expressions for stability criteria. Thus one assumes that the functional form of density and temperature field is the following:

$$T(\vec{r},t) = T_h(t) + \delta T(\vec{r},t), \tag{3.31}$$

$$n(\vec{r},t) = n_h + \delta n(\vec{r},t), \tag{3.32}$$

where $T_h(t)$ and n_h are the homogeneous solutions. The $\delta T(\vec{r},t), \delta n(\vec{r},t)$ terms represent small, temporal and position-dependent perturbations around a homogeneous, time-dependent temperature field and a homogenous, steady density field, respectively. The insertion of (3.31) into the hydrodynamic equations and other assumptions allow to rewrite these equations into a linearized form.

In the next step this linearized form is transformed into Fourier space. This has the advantage that derivations in the position space turn into multipliers in the Fourier space. The definition of a Fourier-transformed field $\mathcal{F}[\vec{a}(\vec{r},t)](\vec{k},t)$ is

$$\vec{a}_{\vec{k}}(t) \equiv \mathcal{F}[\vec{a}(\vec{r},t)](\vec{k},t) = \frac{1}{\sqrt{V}} \int \mathrm{d}\vec{r} e^{-i\vec{k}\cdot\vec{r}} \vec{a}(\vec{r},t). \tag{3.33}$$

Now, it is possible to arrange the linearized form within the Fourier space into the following structure, where $\hat{\mathbf{M}}$ consists only of algebraic combinations of the fields but no derivatives:

$$\frac{\partial \vec{\Psi}}{\partial t} = \hat{\mathbf{M}}\vec{\Psi} \quad \text{with} \quad \vec{\Psi} \equiv \left(n_{\vec{k}} \;\; \vec{u}_{\vec{k}} \;\; T_{\vec{k}}\right)^{\mathrm{T}}. \tag{3.34}$$

Finally, the above equation can be written into an eigenvalue equation and the

eigenvalues $\lambda(\vec{k})$ are obtained by solving the secular equation. If for a value of $\vec{k}$ $\mathrm{Re}(\lambda(\vec{k})) \geq 0$, then the corresponding eigenvector is an unstable mode. Therefore one can calculate a critical $\vec{k}_{\mathrm{crit}}$ where a change of sign occurs and one obtains a stability criterion.

Because of the fact that only modes with $k \geq 2\pi/L$ may exist in the system, there is a connection between stability and system size. Thus the condition for instability is $k_{\mathrm{crit}} \geq 2\pi/L$ if it is the case that $\forall k > k_{\mathrm{crit}} : \mathrm{Re}(\lambda(\vec{k})) \leq 0$. Otherwise k_{crit} would not be the critical size but the largest k^+ for which $k^+ \geq 2\pi/L$ and $\mathrm{Re}(\lambda(\vec{k^+})) \geq 0$ is fulfilled. The dimensioned form of L_{crit} in 2D is:

$$L_{\mathrm{crit}} = \frac{\pi^{3/2}\sqrt{2}\sigma}{\nu 4 g_2(\sigma)} \sqrt{\frac{(\kappa^*(\varepsilon) - \mu^*(\varepsilon))}{\zeta^*(\varepsilon)}}, \tag{3.35}$$

$$g_2(\sigma) = \frac{2-\nu}{2(1-\nu)^3}, \tag{3.36}$$

where $\kappa^*(\varepsilon)$, $\mu^*(\varepsilon)$ and $\zeta^*(\varepsilon)$ exclusively depend on ε. $g_2(\sigma)$ is the pair correlation function at contact of a hard-sphere fluid. As a result, for $L \geq L_{\mathrm{crit}}$, an initially homogenous, flux-free system develops clusters. For $L \leq L_{\mathrm{crit}}$ the system stays stable and therefore homogeneous.

3.7 The homogeneous, steady state

The homogenization is made through a vibration of the container walls, that is, through an external energy supply. Through the wall-oscillation kinetic energy is transferred to the granular gas in vicinity to the walls. Because of the underlying microscopic collision rules this energy transforms into disordered movement [10], that is granular temperature. The generated heated area next to the walls distributes its thermal energy to the rest of the container because of Eq. (3.11).

The entire shaking process is limited in time and arranged so that it leads to a homogeneous, flux-free, free cooling, granular gas after the process is finished. This is because the aim is to generate a starting condition for experiments, which serve to observe the free-cooling state. A homogenous, stimulated system is not part of this thesis.

A requirement for the generated state is that it should be homogenous over at least

an order of magnitude in time and the homogeneity not be a short-lived, random effect with local flows. We will refer to these states as homogeneous, steady states. Below we provide a justification of the usage of a constant ε in the case of vibrating walls.

In [1] an expression for ε in the viscoelastic case is derived:

$$\varepsilon = 1 - c_1 g^{1/5} = 1 - (1 - \varepsilon_0) g^{1/5}, \tag{3.37}$$

$$\propto 1 - (1 - \varepsilon_0) T^{1/10}, \tag{3.38}$$

where g is the impact velocity, c_1 includes material parameters and ε_0 the initial coefficient of restitution for $T(t = 0) = T_0$. The expression $g \propto \sqrt{T}$ is valid because of the absence of local flows.
Suppose a temperature decay after time t' in the form of $T(t') = T_0 10^{-p}, T(t = 0) = T_0 = 1, \varepsilon(T_0) = 0.975$ and define the relative deviation $\Delta\varepsilon \equiv \frac{\varepsilon(T_0) - \varepsilon(T(t'))}{\varepsilon(T_0)}$ to 0.02. With these values, which are also used during the simulations, the maximum permitted value of p is ≈ 6. In other words, if T declines over six orders of magnitudes, then the relative deviation of ε is still smaller then 2 %.

The above explanation that the temperature decay in a shaken system is balanced, is supported through Fig. (5.7). It shows exemplary that the temperature varies merely over two orders of magnitudes during the entire shaking process. Therefore it is justified to use a constant coefficient of restitution in a shaken system.

4 Numerical and technical details

In the whole thesis, a square, two dimensional container, which is divided up in square cells, is considered. The number of cells is fixed to 128^2, the value of the fields in Eq. (3.23)-(3.25) is calculated in each cell. Thus the resolution of the physical quantities is high enough to represent the fields in an appropriate way and low enough to keep computational cost to a reasonable level. This is because higher resolutions increases the computing time. In addition, keeping the amount of cells low saves computer memory. This saved memory can be used to increase the temporal resolution of a simulation, that is to increase the frequency of stored time steps.

Here follows a simple sketch of the finite volume method, which is used to solve the conservative form of the hydrodynamic equations (3.23)-(3.25).

- First of all one choose an initial condition for the conservative variables in the middle of each cell.
- The divergence theorem allows to transform the hydrodynamic equations into surface integrals of the whole container which can be divided up into a sum of surface integrals of each single cell [8].
- These integrals are approximated with the help of the Gaussian quadrature method which uses four sampling points per cubic surface [11].
- To obtain the field values at the sampling points at the very beginning one uses a seventh order WENO interpolation of the initial values.
- In the next step the fluxes between the cells can be approximated by means of a MUSTA scheme and finally one obtains the cells inside values for the next time step. WENO and MUSTA are commonly used numerical methods in computational fluid dynamics and stand for “weighted essentially non-oscillatory”, and “multi stage”, respectively. [12]

Since the numerical simulations are performed with dimensionless quantities, we want to define the relation between the SI units, which are used in the thesis, and the dimensionless units. From this point, we basically use SI units, otherwise it is mentioned explicitly. The general form of the relation is $q_{\mathrm{SI}} = q\hat{q}_{\mathrm{Ref}}$, where q_{SI} is a physical quantity in SI-units, q the dimensionless value and $\hat{q}_{\mathrm{Ref}}$ a reference value.

- space reference: $\hat{x}_{\mathrm{Ref}} = L_{\mathrm{cell}} = \sigma C$,
  where L_{cell} is the length of a single cell in m, σ the particle diameter in m and C a multiplier. The value of σ is set in the following chapter,
- container size (in SI units): $L = \hat{x}_{\mathrm{Ref}}128$,
- time reference: $\hat{t}_{\mathrm{Ref}} = \hat{x}_{\mathrm{Ref}}/v_{\mathrm{th},0}$,
  where $v_{\mathrm{th},0} = 0.1\,\mathrm{m/s}$ is the initial thermal velocity of particles in the absence of local flows,
- temperature reference: $\hat{T}_{\mathrm{Ref}} = mv_{\mathrm{th},0}^2/d = \langle T_{\mathrm{SI}}(0)\rangle$,
  where $d = 2$ is the system dimension and m the mass per particle,
- energy reference: $\hat{E}_{\mathrm{Ref}} = mv_{\mathrm{th},0}^2/2$,
- velocity reference: $\hat{v}_{\mathrm{Ref}} = v_{\mathrm{th},0}$,
- density reference: $\hat{n}_{\mathrm{Ref}} = 4\langle\nu\rangle/(\pi\sigma^2) = \langle n\rangle$.

The source code is written in C and parallelized with CUDA, a programming technique which takes advantage of the architecture of graphic processing units (GPU). Therefore, additional computing capacity is provided. The simulations were made on computers of type Dell R720, with 64 GB RAM, two CUDA-cards (Tesla K20Xm) and two processors (Xeon E5-2650). Each processor consists out of eight cores with a frequency of 2.6 GHz.
16 of those computers were available for the simulations, with a 120 GB hard drive in each case.
The required power during full capacity is about 900 W for each computer. Since all 16 computers are stored in one computer cabinet, the resulting heat emission has to be absorbed by means of a water-to-air cooling.
The data analysis is basically performed with scripts in Matlab and Gnuplot.

5 Preparations

5.1 General system parameter

Here, we introduce the parameters that stay constant during the evolution of a simulation. The wall-gas interaction underlies so called "hard walls", which means that the velocity component is reflected inelastically and the tangential component remains constant. We tune the first set of parameters according to microgravity experiments carried out in suborbital rockets [4]. We do this to find an access point into a multidimensional parameter space. These are:

- particle diameter: $\sigma \propto 10^{-3}\,\mathrm{m}$;
- average packing fraction: $\langle \nu \rangle = 0.02$;
  The packing fraction used in Ref. [4] was ≈ 0.008 but in Chap. (5.5) we justify a minimal packing fraction of 0.02.
- system size: $L_{\mathrm{Sys}} \approx 10\,\mathrm{cm}$.

The choice of ε varies throughout the chapters. When studying the freely cooling of granular gases it is set to 0.975. To solely consider the reference frame in (5.3.2) the cooling of the granular gas is switched off through $\varepsilon = 1$. Finally in Sec. (6.2) ε is set to 0.85, which represents a realistic value for $\gamma - Al_2O_3$ granules [13].

5.2 Freely cooling granular gases

Before we consider inhomogeneous density distributions and influencing them with external forces, we first want to deal with the evolution of initially homogeneously distributed, force-free systems. As mentioned in Chap. (1) these so-called freely cooling granular gases are the subject of recent, experimental research. In Chap. (1)

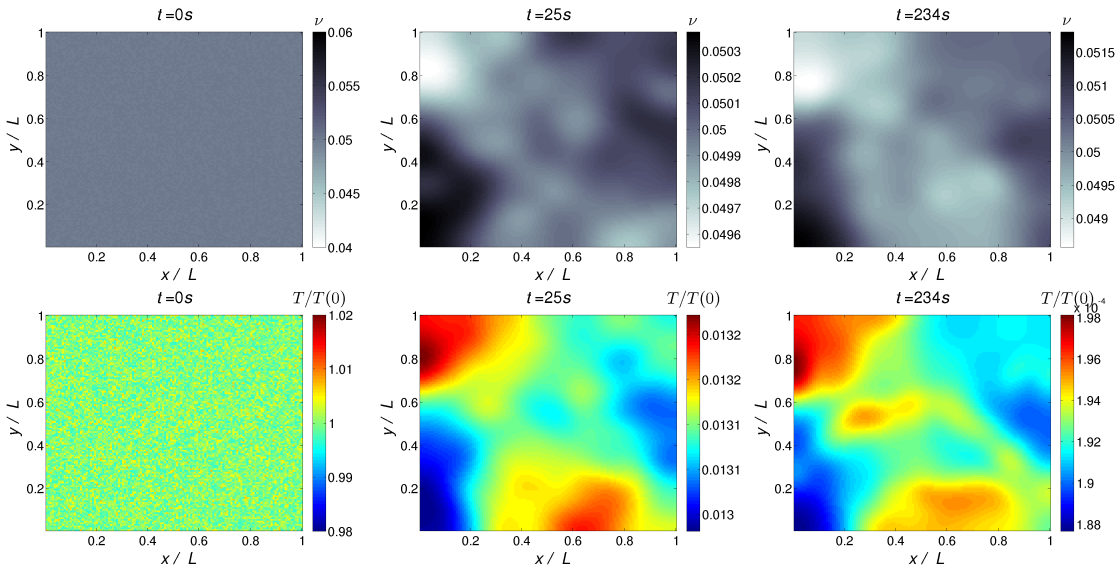

Figure 5.1: The evolution of the density (top row) and temperature (bottom row) in a freely cooling granular gas for $L > L_{\text{crit}}$.

and (3.6) it was already elucidated that these freely cooling granular gases may develop self organized density patterns. According to Sec. (3.6) the occurrence of such a pattern formation depends on the system size L, that is, for systems with $L \leq L_{\text{crit}}$ no patterns appear. In Fig. (5.1) the temporal development of the density with parameters chosen so that $L \geq L_{\text{crit}}$ can be seen.

The distributions of the number density $n(\vec{x}, 0)$ and velocity field $\vec{v}(\vec{x}, 0)$ are chosen randomly with small, realistic fluctuation ranges with $\langle \vec{v}(\vec{x}, 0) \rangle = 0$. One uses these fluctuations in order to avoid numerical errors. These occur due to equal values of the main physical quantities of adjacent finite volumes.
In the whole system the hydrostatic pressure p is initially set to a constant to avoid local mass flows, generated through initial pressure gradients. Thus the initial temperature field is defined through Eq. (3.12) with $p(\vec{x}, t = 0) \equiv \text{const.}$:

$$T \propto \frac{1}{n\left[1 + (1 + \varepsilon) g_{\text{Q}}(\sigma)\nu\right]}. \tag{5.1}$$

The definition of the initial set of variables is completed and the energy density ρE can be calculated according to Eq. (3.22).

The following is a short, descriptive explanation of the structure formation in Fig.

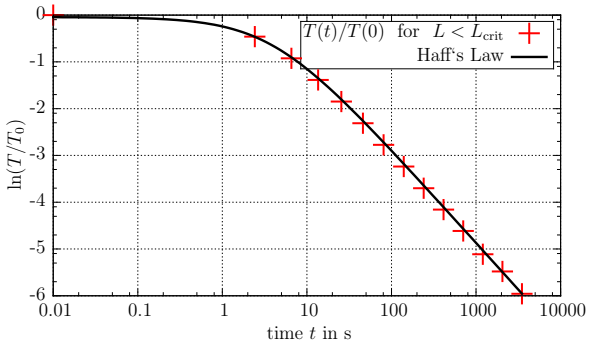

Figure 5.2: Theoretical prediction of Haff's law (black curve) in units of the initial temperature T_0 together with the calculations.

(5.1): The origin of the patterns is due to small, spatial density fluctuations [1]. As already explained in (3.2) in comparison to dilute density regions the collision rate in denser regions is higher. As the energy loss for constant coefficient of restitution merely depends on the total number of collisions, denser regions lose more kinetic energy. Hence the local pressure decays faster in these regions and therefore local flows towards dense regions are generated. This reinforces the effect and leads to a formation of stable clusters.

In Chap. (3.5) Haff's law, a rule for the time dependent change of granular temperature, was derived and is substantiated by means of a typical simulation shown in Fig. (5.2).

5.3 Description of the shaking process

5.3.1 Introduction

The key component of the thesis are the shaking walls. First of all we consider a one dimensional oscillation, which means one pair of opposite walls are moving synchronously and the container volume remains temporarily constant. Here, we define this direction as the $x-$axis in a Cartesian coordinate system. To realize the shaking inside the numerical solver one generates an oscillating force field at the two

opposite ends. This force field has the form

$$\vec{E}(t) = -\vec{A}\cos(2\pi f t + \phi)(2\pi f)^2, \tag{5.2}$$

with spatial constant amplitude $\vec{A} = \begin{pmatrix} A_x \ , \ 0 \end{pmatrix}^{\mathrm{T}}$, frequency f, phase ϕ and time t. This leads to a spatial constant, instantaneous acceleration $\vec{a}(t)$ of the gas within every cell, where $\vec{a}(t) = \vec{E}(t)$. In other words, a centered particle, which does not touch the walls, would be subject to an acceleration $\vec{a}(t)$.
The previous example illustrates that this oscillating gravitational field describes a shaken system in a comoving frame, that is a frame where all walls are at rest. As a consequence the temporal evolution of the kinetic energy and position $\vec{x}$ of the described particle is oscillating.

5.3.2 Shifting the reference frame

Since we are interested in the kinetic energy change transmitted through the walls, that is through wall-particle collisions, we have to switch to an inertial reference frame where the box center remains stationary (for $A < L$) and the walls oscillate. However, for our representations of the position $\vec{x}$ we stay in the accelerated system. Consider an oscillating amplitude larger than the box size, for such a system we find more clear to represent the trajectory of the barycenter relative to resting walls. In the following the transformation of the velocity field, and kinetic energy is listed:

- to achieve the inertial velocity field $\vec{v}_I(\vec{x}, t)$, one has to subtract the spatial constant oscillation velocity $\vec{v}_{\mathrm{wall}}(t)$ of the velocity field in the accelerated frame $\vec{v}_A(\vec{x}, t)$. $\vec{v}_{\mathrm{wall}}(t)$ is defined in (5.8)

$$\vec{v}_I(\vec{x}, t) = \vec{v}_A(\vec{x}, t) - \vec{v}_{\mathrm{wall}}(t) \tag{5.3}$$

- as a consequence $E_{\mathrm{KinI}}(\vec{x}, t)$ results in:

$$E_{\mathrm{KinI}}(\vec{x}, t) = \frac{m}{2}\vec{v}_I(\vec{x}, t)^2. \tag{5.4}$$

5.3.3 Choice of the initial phase

The choice of the phase in $\vec{a}(t)$ (see Eq. (5.2)) follows from the following deliberation. Due to the fact that we start our simulations with a system at rest and afterwards apply an oscillation, the wall velocity v_{wall} and the average gas velocity $\langle\vec{v}\rangle$ at $t = 0$ has to be zero. Since

$$\int \vec{a}(t)\ \mathrm{d}t = -\vec{A}\sin(2\pi f t + \phi)2\pi f = v_{\text{wall}}\ , \tag{5.5}$$

ϕ is determined to be zero. The case $\phi \neq 0$ results in $v_{\text{wall}}(0) \neq 0$ and therefore there is no continuous transition between v_{wall} and $\langle\vec{v}\rangle$. This leads to an acceleration pulse in the direction of the first amplitude. As a consequence the gas receives a total momentum and the barycenter shifts into this direction. For the visualization of this evolution, the barycenter $\vec{R}_M$ of the density field is calculated and its x coordinate R_{Mx} is plotted against time t. We renounce to plot R_{My} because it remains constant in this process. Figure (5.3) compares the cases $\phi = 0$ and $\phi \neq 0$. In order to avoid the barycenter shift we choose $\phi = 0$ throughout the thesis.
The barycenter is defined as

$$\vec{R}_M = \frac{1}{M}\sum_{i=1}^{N} \rho_i \Delta V r_i \tag{5.6}$$

where M is the total system mass, N the total number of cubic cells, ρ_i the mass density in cell i and ΔV the volume of a single cell.

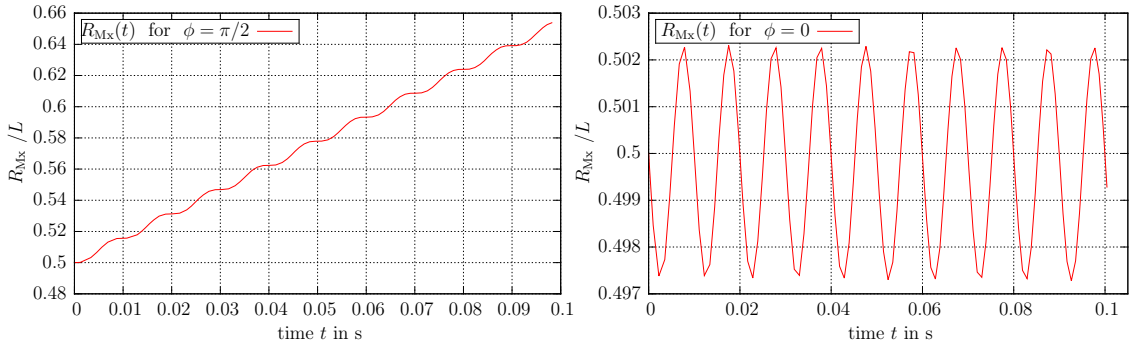

Figure 5.3: The left panel represents the barycenter shift in the accelerated reference frame for $\phi = \pi/2$. In comparison the right plot shows the same case for $\phi = 0$ and an oscillation with constant mean value is apparent.

5.3.4 Measuring the oscillation of a Gaussian density distribution

To substantiate the main statement of Sec. (5.3.1), that one consider an accelerated reference frame, we simulate a physical system similar to a sole particle in a shaken box. The position of the barycenter is centered. Due to the fact that our simulations are based on hydrodynamics we cannot simulate single particles. The appropriate density distribution is the Dirac delta function which can be approximated through a 2D-Gaussian distribution with small standard deviation σ.

Since the walls in x-direction (parallel to the shaking direction) have no friction with the gas, it does not change the wall-gas interaction to confine a 1D-Gaussian distribution with a gradient parallel to the x-axis (see Fig. (5.4)). This has the advantage to reduce areas close to zero in the density field. It is necessary to avoid these areas, because they pose the problem to increase numerical errors which is a common issue in computational hydrodynamics [14, 15]. We tried to keep σ preferable low which means that for decreasing σ the numeric solver is able to deal with the ever declining density values at the border of the box. For the same arguments as in (5.2) to each initial density value a small, random value is added. As in Sec. (5.2) an initially constant hydrostatic pressure and the same initial velocity distribution is chosen. The density distribution ρ_{gaus} can be seen in Fig. (5.4).

Finally the temporal development of the kinetic energy of ρ_{gaus} is considered in the inertial and the accelerated reference frame (see Fig. (5.4)). We observe that the energy oscillation is even present in the inertial system. This can be explained by the fact that there even exists a dilute mass layer in vicinity to the walls which is accelerated and therefore contains the kinetic energy.

5.3.5 Transient and decay procedure

When considering initial states with near-wall densities higher than in the previous chapter, the wall velocity v_{wall} can be better transmitted into the system. This leads to stronger collisions in the middle of the box (see Fig. (5.6)), that is denser regions occur during the collisions. These regions tend to stay dense (see Chap. (5.2)) and it is difficult to dissolve these areas afterwards. In addition to that, the probability of numerical errors rises, due to higher gradients of the physical

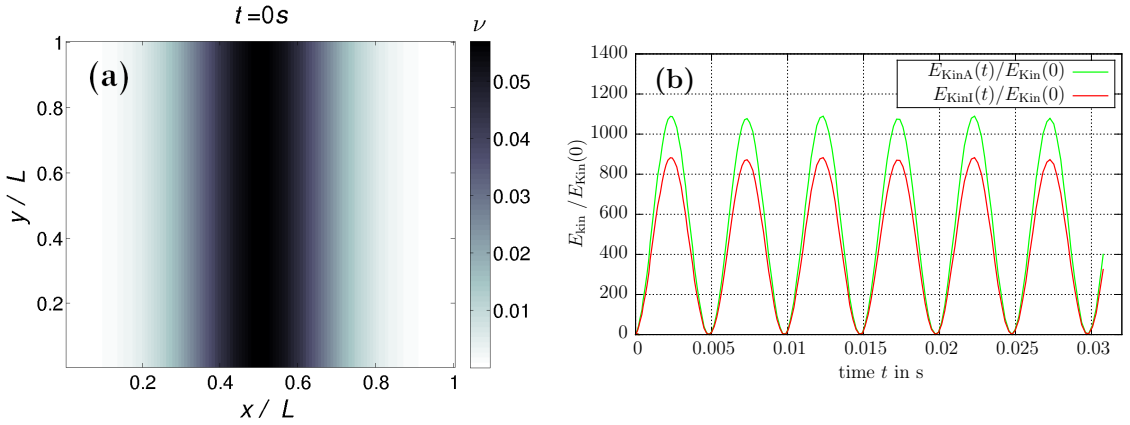

Figure 5.4: (a) The initial 1D Gaussian density distribution ρ_{gaus}. (b) The temporal development of the kinetic energy per particle of ρ_{gaus} in the accelerated reference frame $E_{\mathrm{KinA}}(t)$ and the inertial reference frame $E_{\mathrm{KinI}}(t)$ is shown with parameters $f = 100\,\mathrm{Hz},\ A = 0.14\,\sigma$.

quantities. In order to avoid these kind of effects one has to revise the oscillation procedure. The highest impact of v_{wall} to the system is during the first oscillations, since near-wall mass layers become thinner and further oscillations accelerate lighter mass layers. Because of that it is sufficient to develop a starting procedure which we call "transient procedure".

In order to build a transition from the oscillation process to the freely cooling state, after the inhomogeneous state is dissolved, one has to develop a decay procedure, too. We tried different kinds of transient and decay times and finally figured out that it is quite important to keep v_{wall} in the very first period of time as slow as possible. The following, parabolic functional form of the wall acceleration has appropriate properties:

$$a_{\mathrm{wall}}(t) = -A_x\omega^2\cos(\omega t)\begin{cases}\left(\frac{t}{T_{\mathrm{tr}}}\right)^2 & \text{, for} \quad t \le T_{\mathrm{tr}} \\ 1 & \text{, for} \quad T_{\mathrm{tr}} \le t \le T_{\mathrm{E}} \\ \left(\frac{t-(T_{\mathrm{A}}+T_{\mathrm{E}})}{T_{\mathrm{A}}}\right)^2 & \text{, for} \quad T_{\mathrm{E}} \le t \le T_{\mathrm{E}}+T_{\mathrm{A}} \\ 0 & \text{, for} \quad T_{\mathrm{E}}+T_{\mathrm{A}} \le t\end{cases} \tag{5.7}$$

Where T_{tr} is the end of the transient procedure, T_{E} the beginning of the decay procedure, T_{A} the duration of the decay procedure and $\omega \equiv 2\pi f$. The integration

of Eq. (5.7) with respect to time yields the wall velocity v_{wall} and the wall position x_{wall}, respectively ($v_{\mathrm{wall}}(0) = x_{\mathrm{wall}}(0) = 0$).

$$v_{\mathrm{wall}} = A_x\omega \begin{cases} \frac{2\sin(\omega t)-\omega t[2\cos(\omega t)+\omega t\sin(\omega t)]}{(T_{\mathrm{tr}}\omega)^2} & \text{, for} \quad t \le T_{\mathrm{tr}} \\ -\sin(\omega t) & \text{, for} \quad T_{\mathrm{tr}} \le t \le T_{\mathrm{E}} \\ \frac{2\omega(T_{\mathrm{A}}+T_{\mathrm{E}}-t)[\cos(\omega t)-\omega(T_{\mathrm{A}}+T_{\mathrm{E}}-t)\sin(\omega t)]+2\sin(\omega t)}{(T_{\mathrm{A}}\omega)^2} & \text{, for} \quad T_{\mathrm{E}} \le t \le T_{\mathrm{E}}+T_{\mathrm{A}} \\ 0 & \text{, for} \quad T_{\mathrm{E}}+T_{\mathrm{A}} \le t \end{cases} \tag{5.8}$$

$$x_{\mathrm{wall}} = A_x \begin{cases} \frac{((\omega t)^2-6)\cos(\omega t)-4\omega t\sin(\omega t)+6}{(\omega T_{\mathrm{tr}})^2} & \text{, for} \quad t \le T_{\mathrm{tr}} \\ \cos(\omega t) & \text{, for} \quad T_{\mathrm{tr}} \le t \le T_{\mathrm{E}} \\ \frac{[T_{\mathrm{A}}^2\omega^2+2T_{\mathrm{A}}\omega^2(T_{\mathrm{E}}-t)+\omega^2(T_{\mathrm{E}}-t)^2-4]\cos(\omega t)+3\omega(T_{\mathrm{A}}-t+T_{\mathrm{E}})\sin(\omega t)}{(\omega T_{\mathrm{A}})^2} & \text{, for} \quad T_{\mathrm{E}} \le t \le T_{\mathrm{E}}+T_{\mathrm{A}} \\ 0 & \text{, for} \quad T_{\mathrm{E}}+T_{\mathrm{A}} \le t \end{cases} \tag{5.9}$$

In Fig. (5.5) the normalized wall acceleration $a_{\mathrm{wall}}(t)$, velocity v_{wall} and amplitude x_{wall} are compared.

Another advantage of the transient procedure over a harmonic oscillation process is discussed below. A symmetrical oscillation around the initial position $x_{\mathrm{wall}}(0)$ has the advantage to avoid a transmission of an average momentum to the gas. Otherwise the direction of the first amplitude is singled out and an average momentum is transferred in this direction. A harmonic oscillation process of the form $v(t) = A_x\omega\sin(\omega t)$ with $v(0) = 0$ and $x(0) = A_x$, does not oscillate around its initial position $x(0)$ since the distance $x(T) - x(0)$ is ≥ 0

$$x(T) - x(0) = \int_0^T A_x\omega\sin(\omega t) = A_x(1 - \cos(\omega T)) \geq 0. \tag{5.10}$$

However, a harmonic oscillation of the form $v(t) = A_x\omega\cos(\omega t)$ with $v(0) = A_x\omega t$ and $x(0) = 0$ oscillates symmetrically but in Chap. (5.3.3) we already excluded this kind of oscillation.

Now, we calculate the distance $x_{\mathrm{wall}}(T_{\mathrm{tr}}) - x_{\mathrm{wall}}(0)$ for the revised procedure in

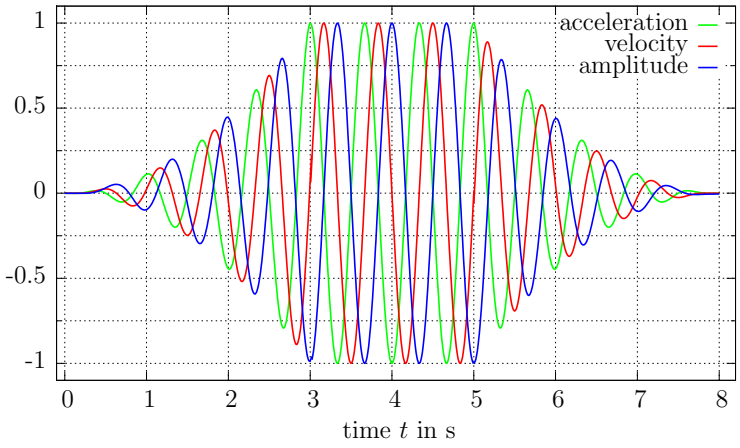

Figure 5.5: The normalized wall acceleration, velocity, and amplitude of the entire shaking process for $T_{\mathrm{tr}} = 3\,\mathrm{s}$, $T_{\mathrm{E}} = 5\,\mathrm{s}$, $T_{\mathrm{A}} = 3\,\mathrm{s}$ and $f = 1.5\,\mathrm{Hz}$ are shown.

Eq. (5.7). Using T_{tr} instead of $T_{\mathrm{E}} + T_{\mathrm{E}}$ is due to the crucial influence of the first oscillations (see beginning of this Sec.).

$$x_{\mathrm{wall}}(T_{\mathrm{tr}}) - x_{\mathrm{wall}}(0) = A_x \left[\cos(\omega T_{\mathrm{tr}}) + \frac{-6\cos(\omega T_{\mathrm{tr}}) - 4\omega T_{\mathrm{tr}}\sin(\omega T_{\mathrm{tr}}) + 6}{\omega^2 {T_{\mathrm{tr}}}^2}\right] \quad (5.11)$$

For $\omega T_{\mathrm{tr}} \gg 1$ the previous expression can be approximated to $A_x \cos(\omega T_{\mathrm{tr}})$, which results into displacements between -A_x and A_x and therefore to a symmetrical oscillation around $x_{\mathrm{wall}}(0) = 0$. A_x is scaling the asymmetrical term, but this occurs for a harmonic oscillation, too (see Eq. (5.10)).

The impact of the transient procedure in terms of the symmetric oscillation, depends on the basic conditions. For example it is negligible, if ρ_{gaus} is the initial condition. On the other hand, in a system that is sensitively dependent on the shaking procedure like in Sec. (6.3) an increasing T_{tr} has a considerable influence on the barycenter (see Fig. (6.12)).

5.4 Critical system size

In Sec. (3.6) a stability criterion for homogeneous, flux-free initial states was given. However we found out that it seems to be valid to actually use this criterion for

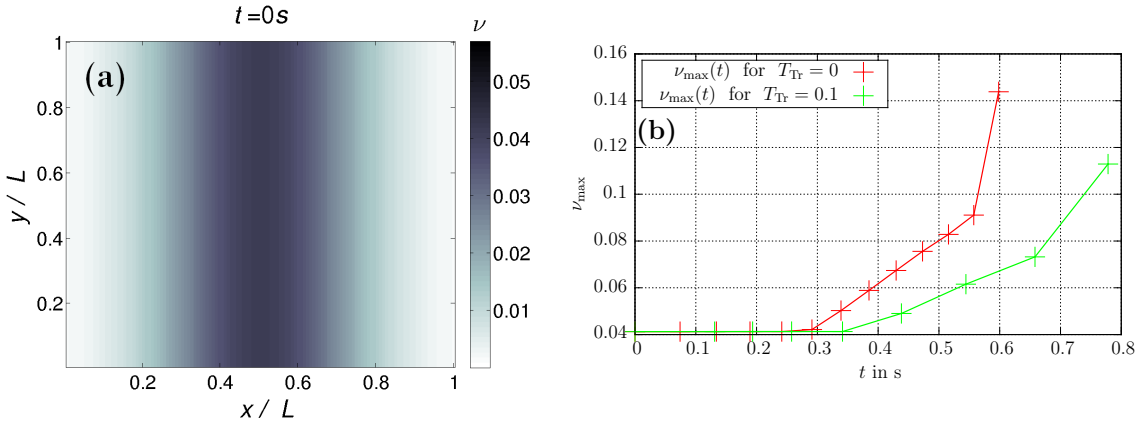

Figure 5.6: (a) The initial Gaussian density distribution with a higher standard deviation σ as in Fig. (5.4) and (b) the temporal evolution of $\nu_{\max}$ for two different transient times T_{tr}.

initially inhomogeneous states with local flows. That means that systems below L_{crit} become completely homogeneous and flux-free. Whereas for $L \geq L_{\mathrm{crit}}$ a collapsing gas can be detected. We proved this statement for systems with different initial density distributions and a variety of initial, local flows. It should be mentioned that the actual value of L differs from the theoretical prediction in Eq. (3.35). For example Eq. (3.35) gives for $\varepsilon = 0.9$ and $\langle\nu\rangle = 0.02$ a critical system size of $50.4\,\sigma$. But even for a $L = 133\,\sigma$ we found states that homogenized by its own. Only in simulations with system sizes above $534.4\,\sigma$ a collapsing occurred (Fig. (5.9)). To find out whether a system is in fact above the actual critical system size we analyzed the standard deviation SD of the density of a freely cooling state of an initially inhomogeneous distribution with SD(ν). If it grows larger than the initial SD, then $L > L_{\mathrm{crit}}$ and otherwise $L < L_{\mathrm{crit}}$. SD(ν) is a measure of the inhomogeneity of the system.

In order to generate different kind of local flows, we oscillate the container with different frequencies and system sizes according to the procedure in (5.3.5). Figure (5.7) shows the L-f phase diagrams for $L \leq L_{\mathrm{crit}}$. The main result is that after the oscillation procedure finished and a local flow was generated, all systems below L become homogenous and flux-free. This can be seen in Fig. (5.7), which shows the typical evolution of the average kinetic energy per particle, a measure for local flows. In Fig. (5.8) to (5.10) some exemplary snapshots of the density- and pressure

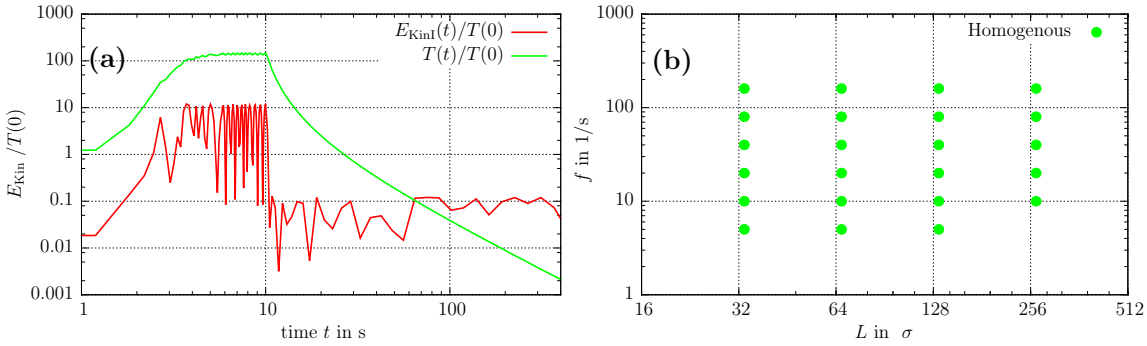

Figure 5.7: (a) A typical evolution of the average kinetic energy per particle E_{Kin} and temperature T during the shaking procedure ($t < 10\,\mathrm{s}$) and afterwards. (b) A f-L phase diagram. In both figures is $L < L_{\mathrm{crit}}$.

fields for both $L \leq L_{\mathrm{crit}}$ and $L \geq L_{\mathrm{crit}}$ are depicted.

5.5 The initial state

In this section we want to focus on the inhomogeneous state inside the two dimensional box that is to be dissolved through vibrating walls.
One could choose different types of inhomogeneous initial states:

- **prescribed states**, one choose a functional form for the velocity, temperature and density fields. Some examples are already given in the previous chapters, e.g. a two dimensional Gaussian density distribution with constant pressure.
- **sedimented states**, that is, one simulates an initially homogenous gas with gravity acceleration over a period of time. After the starting sedimentation reaches a certain maximum density at the bottom of the box, one stops the simulation and use the last state as initial state for the shaking process. Obviously the gravity force is turned off after the energy injection through vibrating walls starts.

During the whole process of the Bachelor thesis we had to deal with numerical problems caused by high gradients among others. This leads to an abortion of the simulations. Nevertheless, to minimize the occurrence of numerical errors we decided

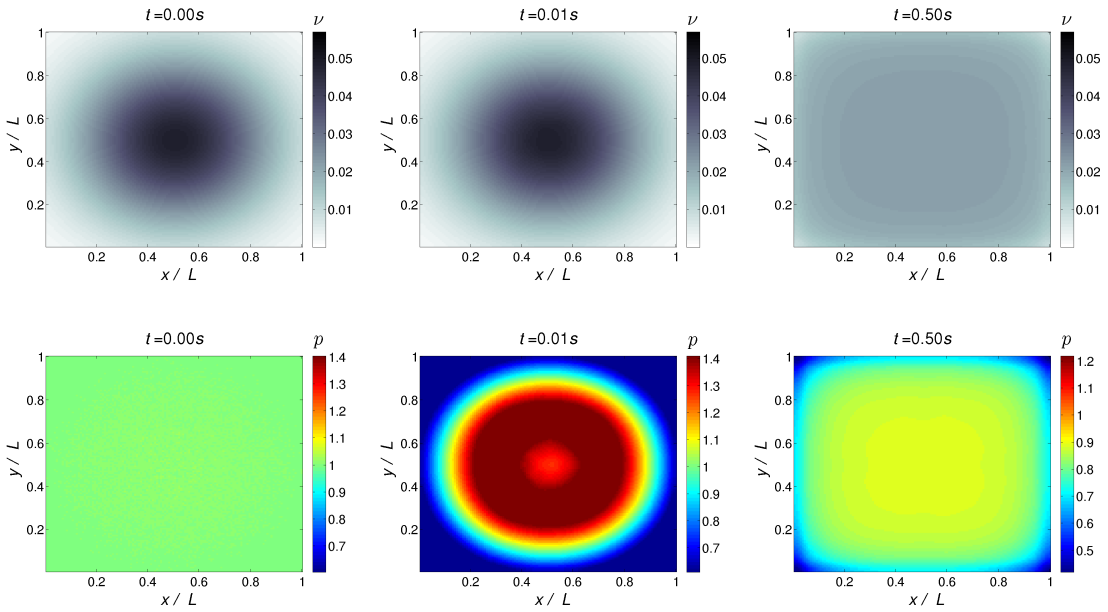

Figure 5.8: The self-organized homogenization of the density field (top row) in a freely cooling granular gas starting with a initially Gaussian density distribution and $L < L_{\text{crit}}$. The bottom row represents the corresponding pressure fields in units of the initial pressure.

to use a prescribed starting state where the single fields can be changed simply and the gradients be adopted. Additionally, sedimented states are difficult to control and even tend to collapse further after the gravity force is turned off.

The functional form of a density distribution with a linear gradient m proved to be appropriate. Because of the fact that areas whose density is close to zero cause numerical problems (see Chap. (5.3.4)), the thinnest density area was set to a fixed value c. This value is chosen in a way that it is large enough to minimize numerical errors and small enough to still receive a distinct gradient. Since we varied the average packing fraction $\langle\nu\rangle$ in the box, c limits a minimal $\langle\nu\rangle$. Finally, the functional form of ν is:

$$\nu(y) = c + my = c + \frac{2(\langle\nu\rangle - c)}{L}y \tag{5.12}$$

For our simulations we used $c = 0.01$ and a minimal $\langle\nu\rangle_{\text{min}} = 0.02$ throughout. With that choice the above constraints are fulfilled and the packing fraction distribution with the minimal possible gradient still goes from 0.01 to 0.03. In other words the

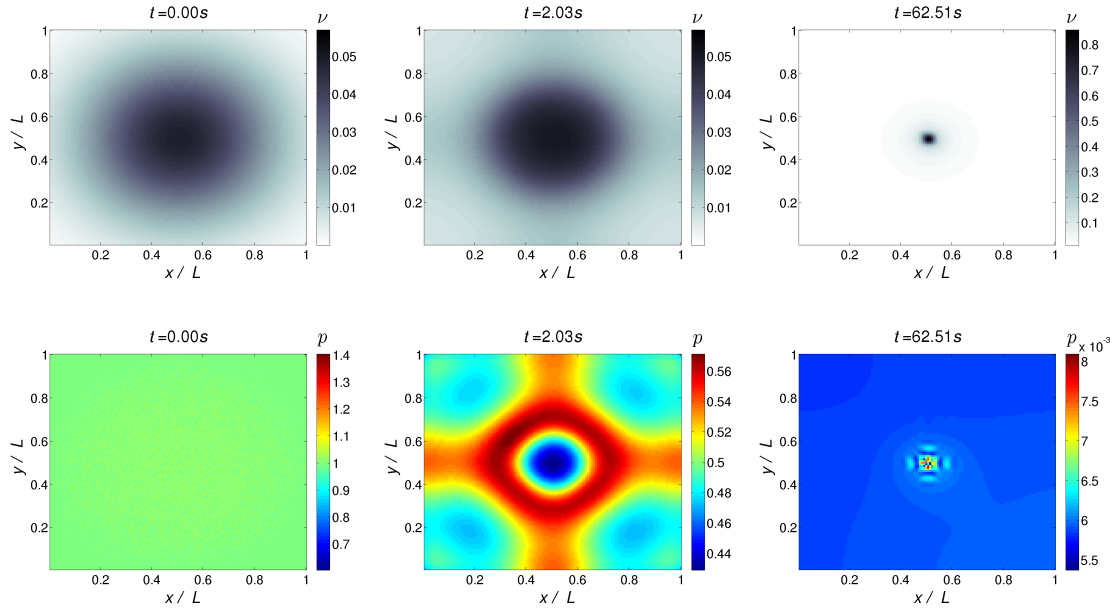

Figure 5.9: The evolution of the density and pressure fields with the same parameters as an in Fig. (5.8) but $L > L_{\text{crit}}$.

densest regions are still three times larger than the thinnest and therefore counts as a distinct inhomogeneous system. Finally as in Sec. (5.2) to each density value a small, random value is added, the distribution of the velocity field is the same and the initial pressure field is constant, too. Due to the result of Sec. (5.4) that for all $L < L_{\text{crit}}$ a self-organized homogenization occurs, we choose $L > L_{\text{crit}}$ and try to dissolve the initial inhomogeneities in the following chapters. For the minimal $\langle\nu\rangle_{\text{min}}$ we therefore set the minimum L to $285\,\sigma$. The pressure and density field of such an initial state can be seen in the left side of Fig. (5.10).

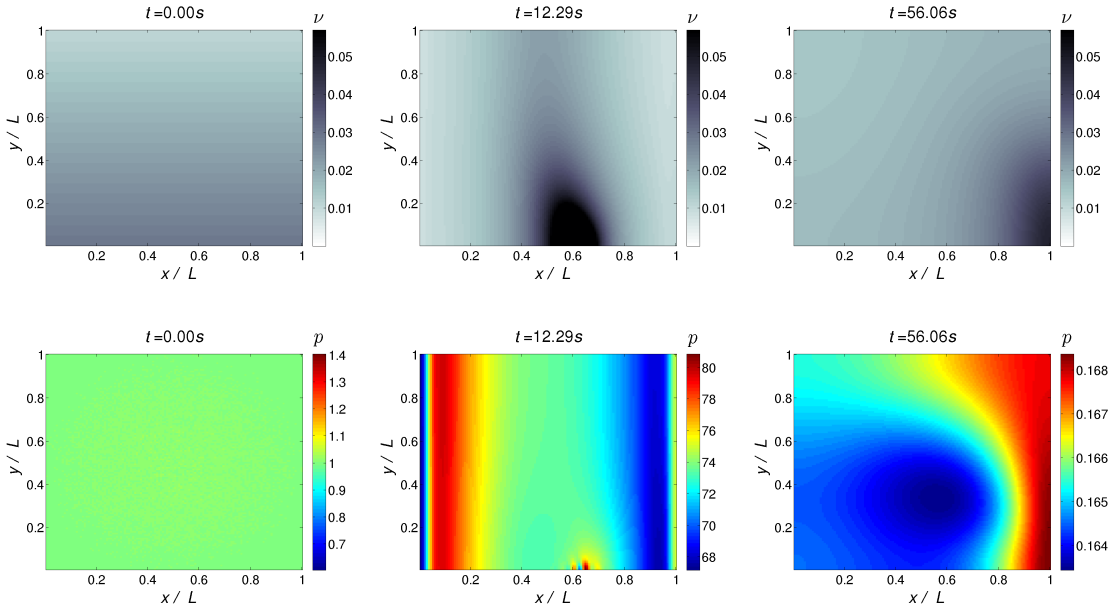

Figure 5.10: Snapshots of the density (top row) and pressure fields (bottom row) before the shaking process ($t = 0$), at the end of the shaking process $t = T_\mathrm{E} + T_\mathrm{A}$, and the beginning self-organized homogenization ($t = 56\,\mathrm{s}$) for $L < L_\mathrm{crit}$.

6 Results

6.1 Shaking perpendicular to the density gradient

Now we focus on how to dissolve the initial state from Fig. (5.10) by shaking in a direction perpendicular to the density gradient (see Fig. (6.1)). As in Fig. (5.7) the

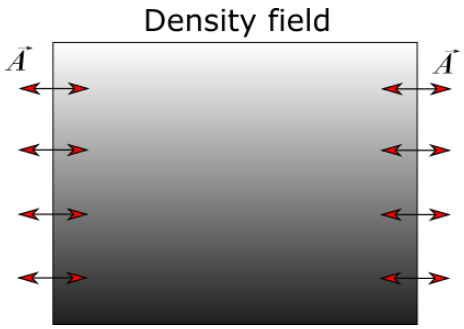

Figure 6.1: Sketch of the system when shaking the 2D container perpendicular to the density gradient.

f-L phase diagram in Fig. (6.2) presents an overview of the parameters we varied. No combination of f and L produced a homogeneous state. A typical development of the density field for the performed simulations can be seen in Fig. (6.3). "Typical" means that almost every simulation evolved in a similar way and finally reached densities too large for the algorithm to handle. These issues are due to very high local packing fractions and pressures, and the limited resolution of the fields. Figure (6.3) (c)-(d) represents one of the few cases where we obtained results after the shaking procedure is over and demonstrates that the resulting dense region tends to build a stable cluster with $\nu_{\max} = 0.88$.

Considering different simulations with constant frequency and variable container size, the density of layers moving to the middle of the container increases. This

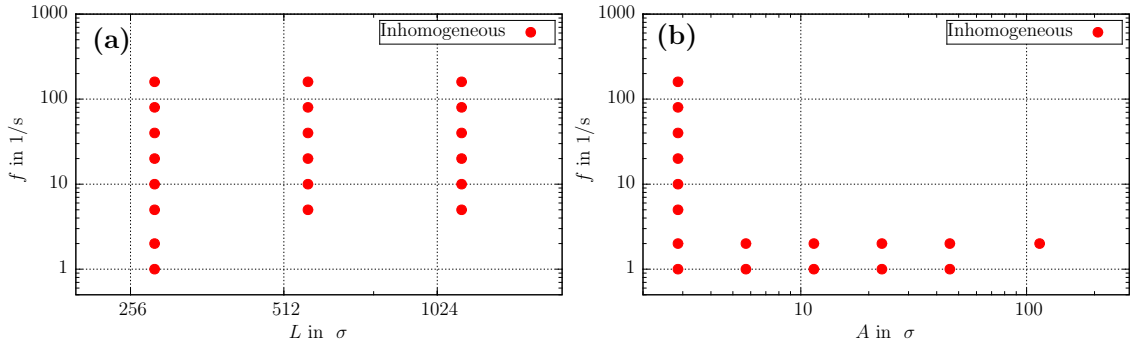

Figure 6.2: (a) The f-L phase diagram with $A = 2.9\,\sigma$ and $\langle\nu\rangle = 0.02$ does not exhibit phase-points in the examined area where the gas becomes homogeneous. (b) The f-A phase diagram with $L = 285\,\sigma$.

is due to the fact that the total system mass rises for increasing system size at constant packing fraction. As mentioned before these denser layers tend to generate numerical errors which lead to abortions and therefore we were not able to even consider the collision of the layers. These layers can be seen in the upper row of Fig. (6.3). Therefore our research was limited to maximum average packing fractions of 0.02 and maximum system sizes of $571\,\sigma$.

In Fig. (6.4) simulations with different frequencies are compared. These simulations aborted short after the collision of the layers when the shaking process was still ongoing. The decrease of the standard deviation SD(ν) of the density and the decrease of the maximum packing fraction $\nu_{\max}$ is due to an expansion directly after the collision. This temporarily, small expansion is a result of the compression but the gas is still kept centered through the vibrating walls and does not lead to an expansion over the whole container (see Fig. (6.3) (c)-(d)). It is striking that the frequency merely influences the temporal development of the system, that is a shifting of the graphs along the t-axis while SD(ν) and $\nu_{\max}$ are hardly affected.

To find out whether the amplitude changes the development of the density field, we varied the parameters according to the f-A phase diagram in Fig. (6.2). Unfortunately it was only possible to show the area for relatively small values of the product fA, because of problems of the stability of the simulations. This is because the value fA scales the amplitude of the wall velocity which leads to large gradients of the physical quantities. Nevertheless, as already explained, the frequency is not a crucial parameter and the limited f-A phase diagram yields probably the main

information.

All in all, since we did not obtain the desired results with the used sets of parameters, we decided to change the orientation between shaking direction and density gradient.

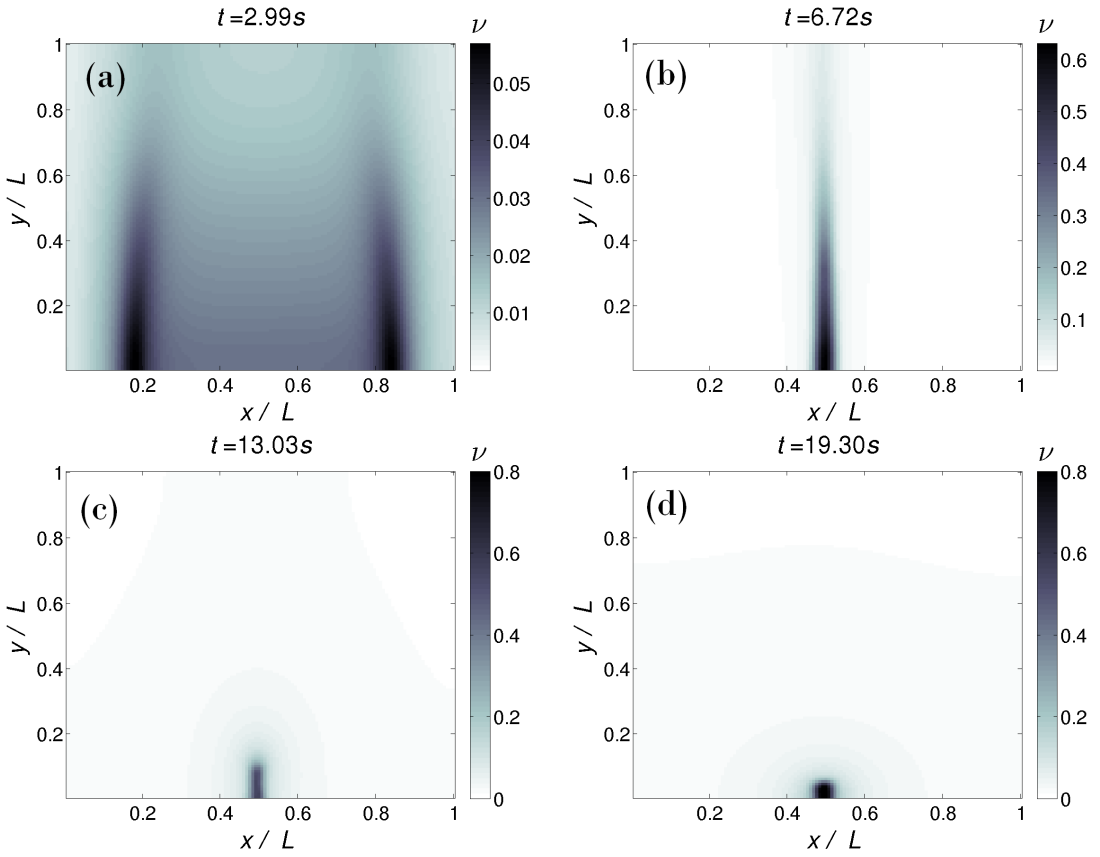

Figure 6.3: (a), (b): A typical evolution of the density field in the event of the perpendicular acceleration with the final collision of the layers and the abortion at $t = 7\,s$. (c), (d): Snapshots of the density fields at the end of the shaking process $t = T_\mathrm{E} + T_\mathrm{A} = 13\,\mathrm{s}$ and the further collapsing afterwards ($t = 19\,\mathrm{s}$). Parameters (a),(b): $L = 571\,\sigma$, $f = 10\,\mathrm{Hz}$, $A = 2.9\,\sigma$, $\langle\nu\rangle = 0.02$; (c),(d): $L = 285\,\sigma$, $f = 2\,\mathrm{Hz}$, $A = 11.4\,\sigma$, $\langle\nu\rangle = 0.02$.

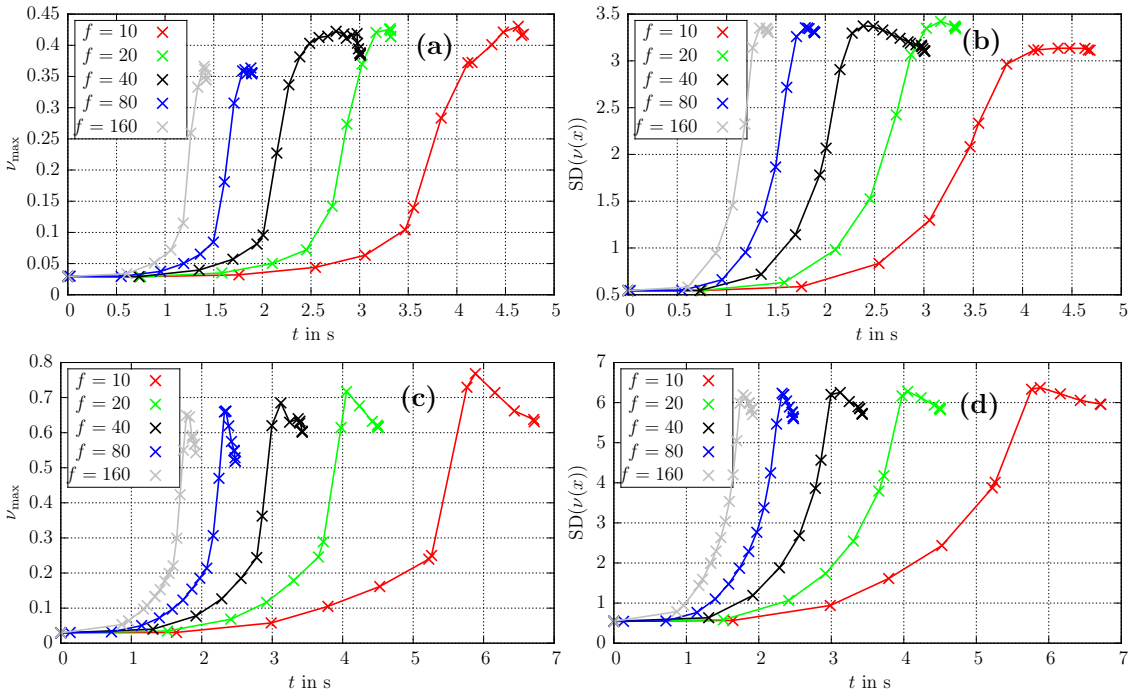

Figure 6.4: The illustration of the impact of the frequency f in Hz on the evolution of the maximum packing fraction $\nu_{\max}$ (a), (c) and the SD(ν) (b), (d). Parameters: $L = 285\,\sigma$ for (a) and (b), $L = 571\,\sigma$ for (c) and (d).

6.2 Shaking parallel to the density gradient

As explained in Sec. (6.1) in order to avoid the generation of dense, stable regions (Fig. (6.3)(d)) and to keep the total mass low, we chose $\langle\nu\rangle = 0.02$ and $L = 285\,\sigma$ which is close to L_{crit}, but still large enough to lead to a distinct self-organized collapsing of the initial state as in Fig. (5.9).
The shaking procedure leads to a collecting of the mass in one single layer in the center of the system, which is symmetric about the x-axis (Fig. (6.8)). During the shaking process its center of mass bounces in the middle of the box, perpendicular to the shaking walls (see Fig. (6.6)). After the oscillation process is over, this layer starts to expand over the whole system.

The position of the dense layer inside the box after the oscillation procedure finishes, determines the evolution of the system. This means the middle layer expand around its barycenter and therefore an off-centered layer leads to an inhomogeneous density distribution (Fig. (6.9)). Varying the duration of the shaking procedure, for

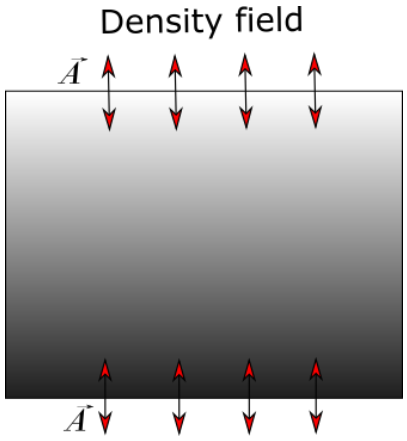

Figure 6.5: Sketch of the system when shaking the 2D container parallel to the density gradient.

constant f and A in a way that the layer stays as centered as possible leads finally to a homogeneous state. This behavior for $f = 10\,\mathrm{Hz}$, $A = 2.9\,\sigma$ is represented in Fig. (6.8). Whether such an evolution towards a homogeneous state occurs, is sensitively dependent on the duration of the transient procedure. For example the two sets of oscillation parameters $T_{\mathrm{E1}} = 6.15\,\mathrm{s}$ and $T_{\mathrm{E2}} = 6.8\,\mathrm{s}$ with constant remaining $T_{\mathrm{tr1}} = T_{\mathrm{A1}} = T_{\mathrm{tr2}} = T_{\mathrm{A2}} = 1\,\mathrm{s}$ generate a homogenous and inhomogeneous state, respectively (see Fig. (6.8) and (6.9)).

For larger system sizes and constant $\langle\nu\rangle$ this expanding of the middle layer disappeared (see Fig. (6.7)). This is due to the fact that the density of the centered layer increases which leads to a stable compacted region. This effect was already treated in Chap. (6.1). Reducing the total mass of the system $M \propto \langle\nu\rangle L^2$, might avoid the occurrence of dense regions. Since $\langle\nu\rangle$ cannot be reduced due to numerical reasons one has to reduce L. To fulfill $L > L_{\mathrm{crit}}$, L_{crit} has to be reduced through an increasing $\langle\nu\rangle$ (see Eq. (3.35)). As a result for decreasing L and $L\langle\nu\rangle = \mathrm{const.}$, one obtains the desired reduced system mass. But in the simulations this does not achieve the required result and actually leads to even denser layers (see green curves in Fig. (6.7)). That is why only the case $\langle\nu\rangle = 0.02$ and $L = 285\,\sigma$ is considered.

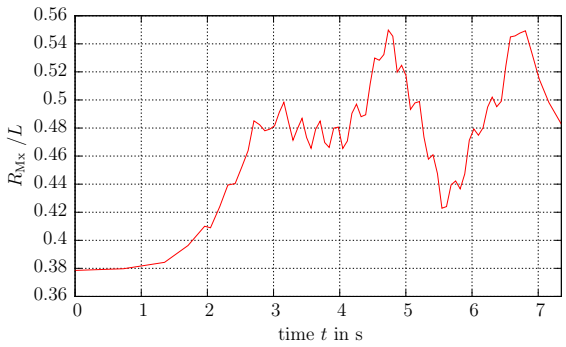

Figure 6.6: Typical evolution of the position of the barycenter R_{My} during the vibration process.

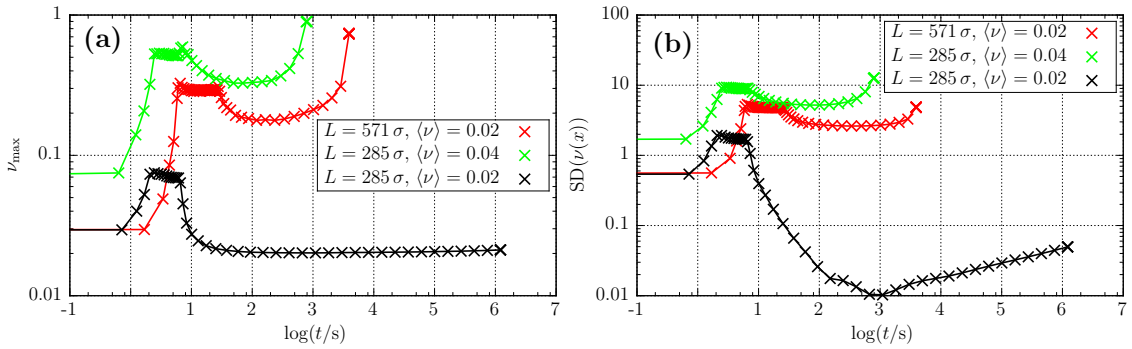

Figure 6.7: Evolution of $\nu_{\max}$ (a) and SD(ν) (b) for three different sets of parameters and appropriate T_{E}. Only the black curves represent a homogenization.

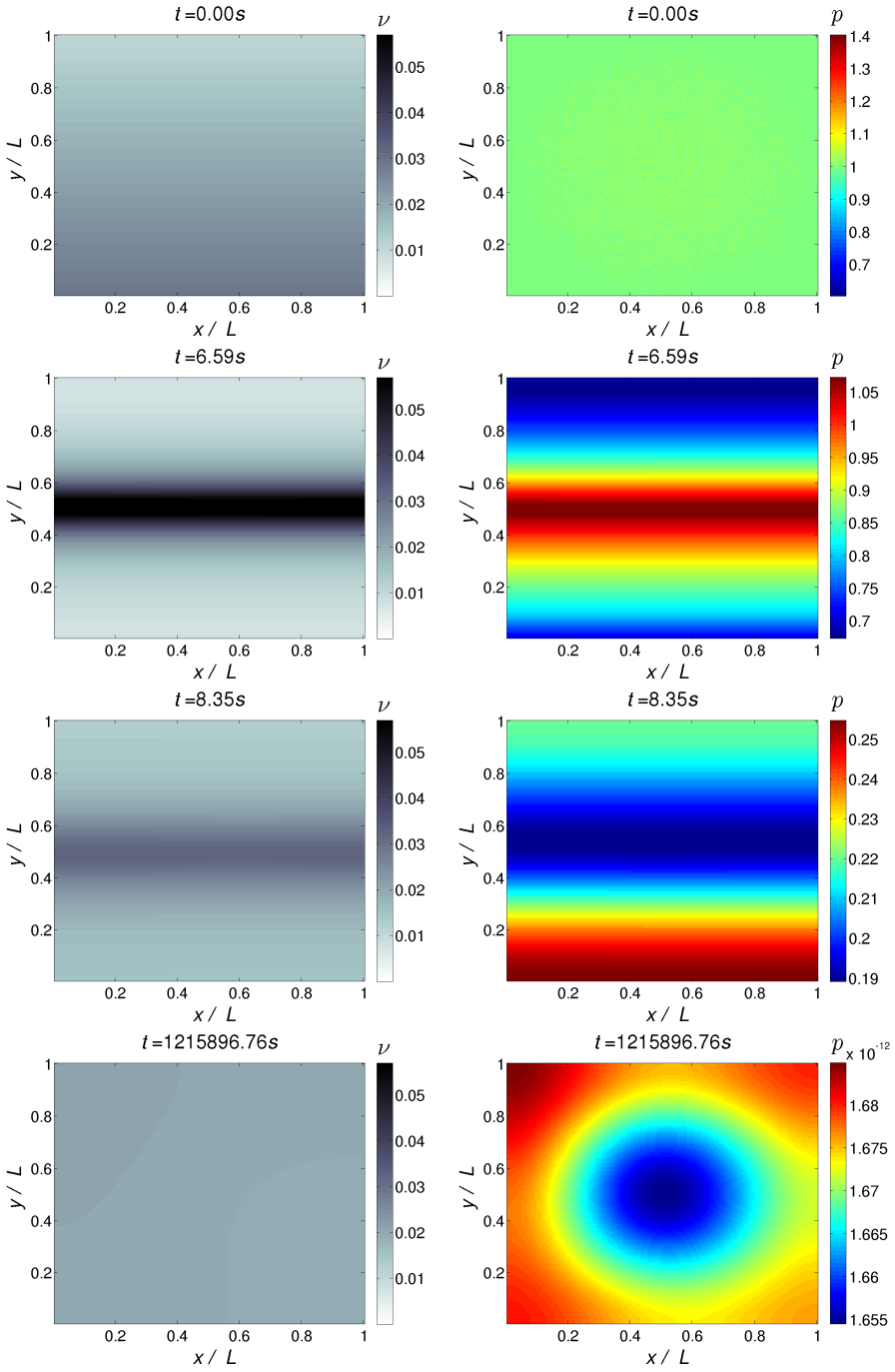

Figure 6.8: The homogenization of the density field (left column) for a centered barycenter at $t = T_\mathrm{E}+T_\mathrm{A} = 7.15\,\mathrm{s}$ and the related pressure fields in units of the initial pressure (right column). Parameters: $L = 285\,\sigma$, $f = 10\,\mathrm{Hz}$, $A = 2.9\,\sigma$, $\langle\nu\rangle = 0.02$ and $T_\mathrm{tr} = T_\mathrm{A} = 1\,\mathrm{s}$

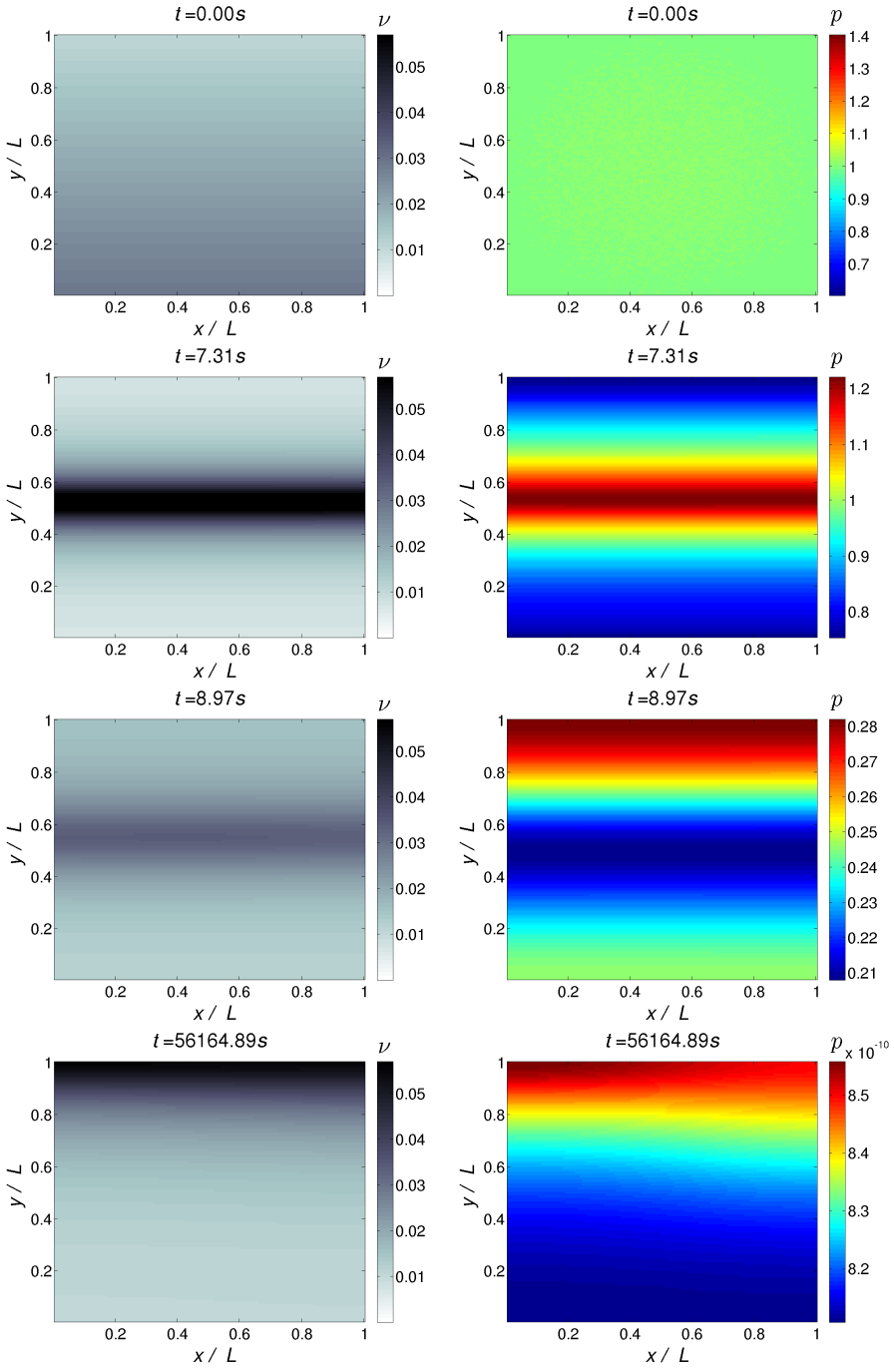

Figure 6.9: The evolution of the density field (left column) for an off-centered barycenter at $t = T_\mathrm{E} + T_\mathrm{A} = 7.8\,\mathrm{s}$ and the related pressure fields (right column) in units of the initial pressure. Parameters: $L = 285\,\sigma$, $f = 10\,\mathrm{Hz}$, $A = 2.9\,\sigma$, $\langle\nu\rangle = 0.02$ and $T_\mathrm{tr} = T_\mathrm{A} = 1\,\mathrm{s}$

6.2.1 Varying f and A

As we found out in Sec. (6.1) that f strongly influences the temporal development of a system one tried the approach $T_i = n_i/f$ in order to produce comparable evolutions for different f. The index i represents one of the three parts of the oscillation procedure and n_i is the number of oscillations that is kept constant when varying f. We already found that the values $n_{\mathrm{tr}} = n_{\mathrm{A}} = 10$ and , $n_{\mathrm{E}} = 61.5$ lead to a homogeneous state for $f = 10\,\mathrm{Hz}$ and $A = 2.9\,\sigma$.

The main result is that this approach actually leads to comparable evolutions and homogeneous states. As in Sec. (6.1) the frequency basically influences the temporal development of the system and $\mathrm{SD}_{\mathrm{max}}$, ν_{max} increase slightly for rising f.
To prove this, the temporal dependence of ν_{max}, R_y, and $\mathrm{SD}(\nu)$ for several frequency is depicted in Fig. (6.10). The slight increase of $\mathrm{SD}(\nu)$ after its minimum also occurs in the free-cooling state and is due to the gradually beginning clustering.

Varying A at constant f and n_i leads to a different position of the barycenter after the oscillation process is finished. It is striking that this barycenter shift stays comparable for arbitrary frequency and fixed n_i (see Fig. (6.10)). As a consequence, adapting n_i in a way the barycenter is centered at $t = T_{\mathrm{E}} + T_{\mathrm{A}}$, leads to homogenous systems in the examined frequency range $[1, 160]\,\mathrm{Hz}$. Nevertheless, this procedure has the disadvantage that it simply dissolves the inhomogeneities that are symmetrical in one direction. To study a more general procedure, which is independent of the initial state we discuss a different shaking protocol in the following chapter.

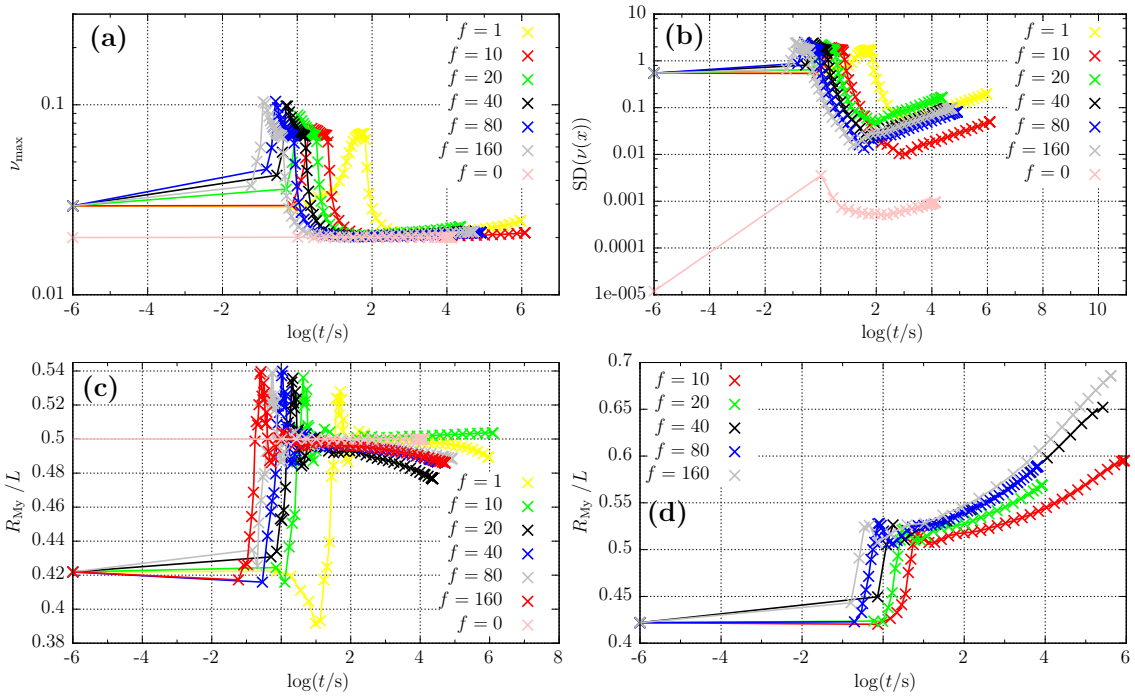

Figure 6.10: The illustration of the impact of the frequency f in Hz on the evolution of the maximum packing fraction $\nu_{\max}$ (a), the standard deviation SD(ν) of the density (b) and the barycenter R_{My} (c). Parameters: $L = 285\,\sigma, \langle\nu\rangle = 0.02, A = 2.9\,\sigma$. (d) The barycenter shift for a changed amplitude $A = 1.4\,\sigma$, varied frequency and otherwise equal parameters.

6.3 All-sided vibration

We now discuss a shaking protocol where all walls vibrate with equal frequency and amplitude. As in Sec. (6.1)-(6.2) the container volume remains temporarily constant. An occurrence of a gravitational force in a certain direction would require pairwise independent shaking walls, but here it is not necessary. As mentioned in Sec. (5.1) hard walls are implemented and the velocity components tangential to the walls remain unchanged. As a result a gas layer close to an arbitrary wall solely achieves an acceleration perpendicular to that wall and the entire gas is pushed to the center (see Fig. (6.13)). To obtain a homogenous state the process described in the previous Chap. is used. Therefore one starts with constant f and A and vary T_E until one obtains a homogenous state. As before one starts with $A = 2.9\,\sigma$ and define $f = 2\,\mathrm{Hz}$.

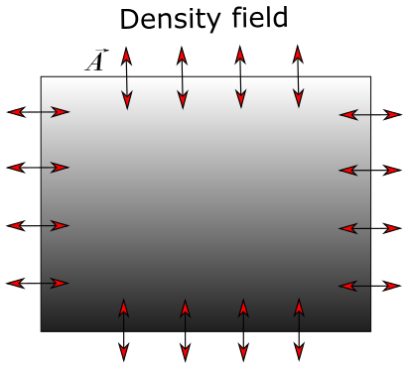

Figure 6.11: Schematic of the system in the all-sided vibrated case.

We vary T_E in a range that it is always large enough so that the barycenter is stabilized in the center at $T_E + T_A$. By stabilized we mean that its momentum is approximately zero. Figure (6.12) shows the results. Every evolution leads to a highly compacted area in the middle that starts to expand at approximately $t = 20\,\mathrm{s}$, that is independent of T_E. Unfortunately most simulations aborted shortly after the expansion and therefore we were not able to examine whether this expansion finally leads to a homogenous state like in Sec. (6.2). This is because it could also be possible that the expansion stops at a certain point. This case arises for a simulation with $T_E = 22.5\,\mathrm{s}$ (see orange curves in Fig. (6.12)). The expansion is merely temporary and its maximum ν evolves towards one, after the shaking process is terminated. This is comparable to the results in Sec. (6.1).

Nevertheless, in order to actually see a homogenous distribution, one has to avoid these abortions. Therefore we tried quite small values of T_E, which has the advantage that $\nu_{\max}$ and $\mathrm{SD}(\nu)$ actually decrease and therefore the simulation stability rises. The downside is that the barycenter is still moving towards the center at $T_E + T_A$ or its location is not stabilized in the center. As in the previous Sec. we find that off-centered expansions do not lead to homogenous state (see for example Fig. (6.14)). The sensitive dependence of $R_M(x, y)$ on T_E which we already noticed in the previous Sec. is even higher.

A method to increase the stability of R_M is, according to Sec. (5.3.5), to raise $T_{\mathrm{tr}} f = n_{\mathrm{tr}}$ and to decrease A. A comparison between different T_{tr} can be seen in Fig. (6.12) (d) and the transient procedure proves to have an impact on the stability. Finally, we find that for the values $A = 0.14\,\sigma$, $n_{\mathrm{tr}} = 100$, $f = 20\,\mathrm{Hz}$ and $T_E = 11.9\,\mathrm{s}$ a homogenous state can be successfully produced, as shown in Fig. (6.13).

The largest advantage of shaking in both directions is that it does not fail for a different symmetry in the initial state. To demonstrate this, the initial density gradient was rotated by 45 °. After adjusting the parameters of the driving protocol we finally obtained a homogenous state, too (see Fig. (6.15)).

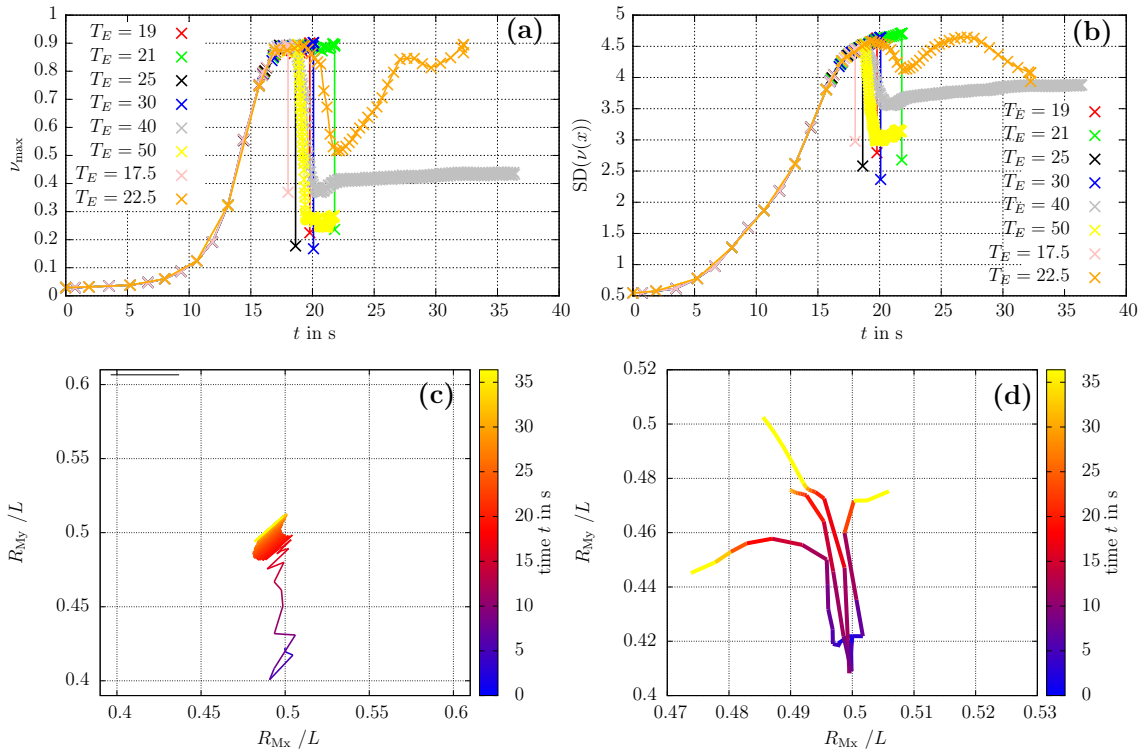

Figure 6.12: The evolution of $\nu_{\max}$ in (a), SD(ν) in (b) in a all-sided vibrated box with stabilized barycenter $R_M(x, y)$ for different values of T_{E} (in s). (c) A typical evolution of the barycenter of such a simulation. (d) illustrates the stabilizing effect of n_{tr}. The middle two trajectories result from $n_{\mathrm{tr}} = 100$, the external from $n_{\mathrm{tr}} = 10$ and otherwise equal parameters.

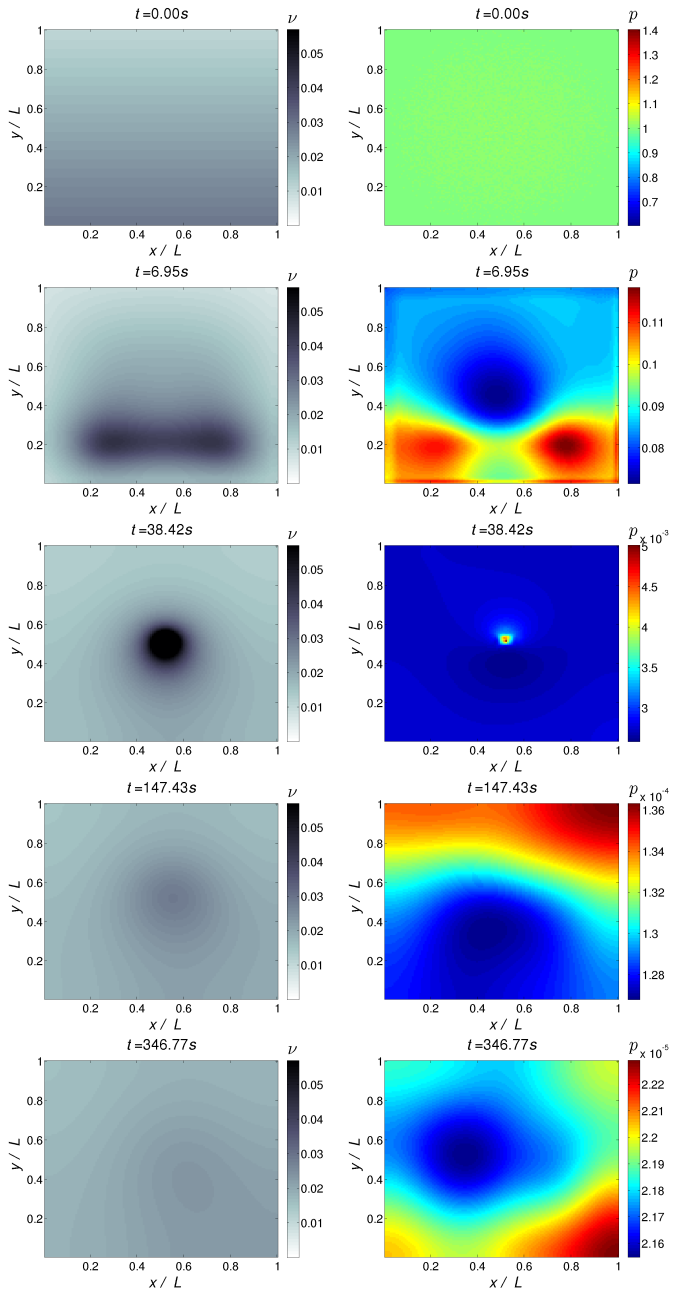

Figure 6.13: The homogenization of the density (left column) for a centered expansion and the related pressure fields in units of the initial pressure (right column). Parameters: $L = 285\,\sigma, \langle\nu\rangle = 0.02, f = 20\,\mathrm{Hz}, A = 0.14\,\sigma, T_{\mathrm{tr}} = T_{\mathrm{A}} = 5\,\mathrm{s}$ and $T_{\mathrm{E}} = 11.9\,\mathrm{s}$

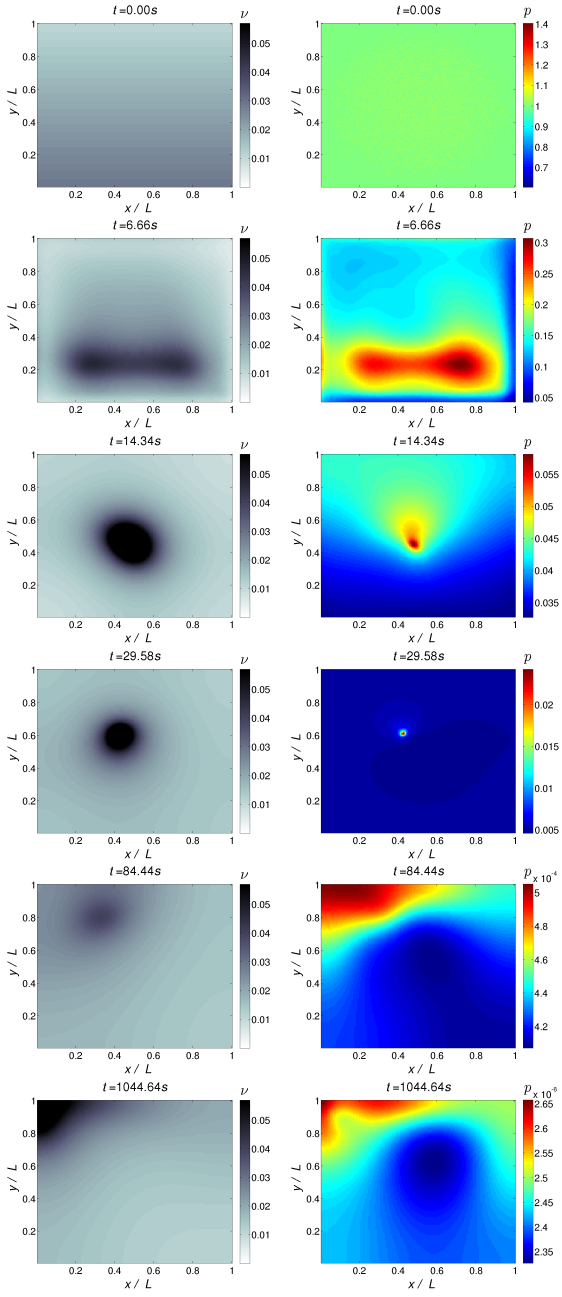

Figure 6.14: The evolution of the density (left column) for an off-centered expansion can be seen and the related pressure fields (right column). Parameters: $L = 285\,\sigma, \langle\nu\rangle = 0.02, f = 20\,\mathrm{Hz}, A = 0.14\,\sigma,\ T_{\mathrm{tr}} = T_{\mathrm{A}} = 5\,\mathrm{s}$ and $T_{\mathrm{E}} = 11.3\,\mathrm{s}$

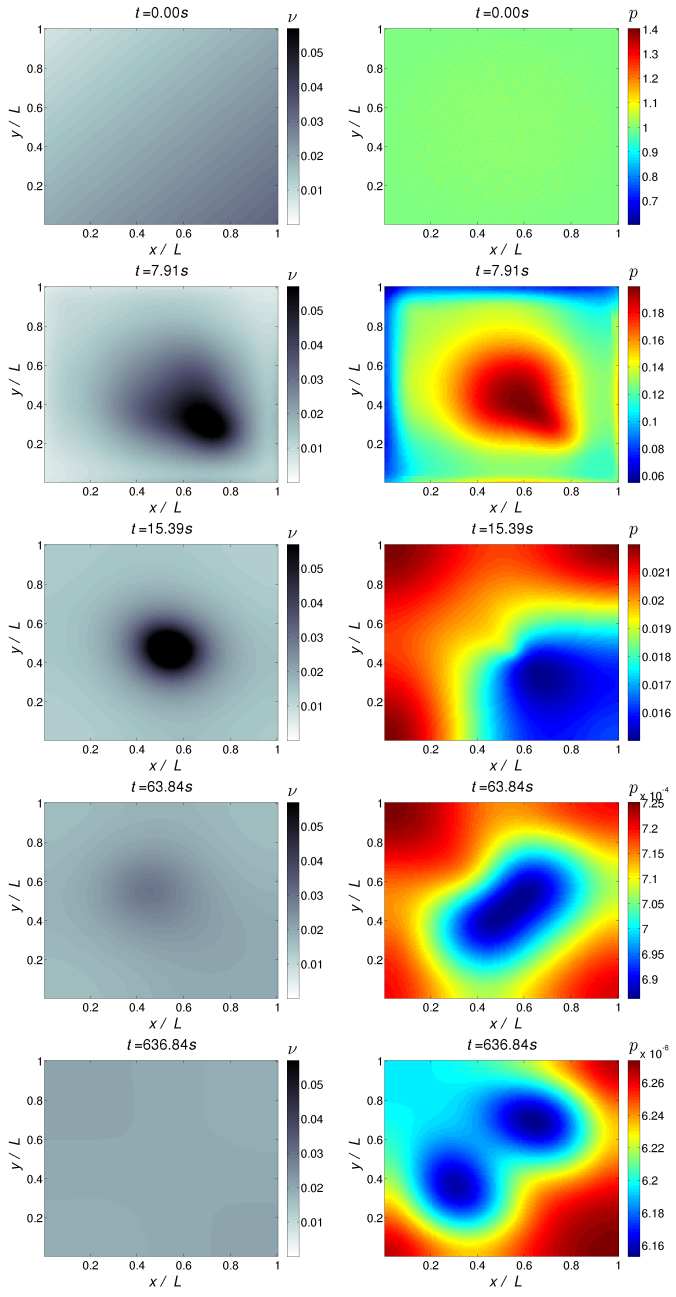

Figure 6.15: Even a different initial symmetry in the density field can be dissolved (left column) and the related pressure in the right fields (right column). Parameters: $L = 285\,\sigma, \langle\nu\rangle = 0.02, f = 2\,\mathrm{Hz},\ A = 2.9\,\sigma,\ T_{\mathrm{tr}} = T_{\mathrm{A}} = 5\,\mathrm{s}$ and $T_{\mathrm{E}} = 7.5\,\mathrm{s}$

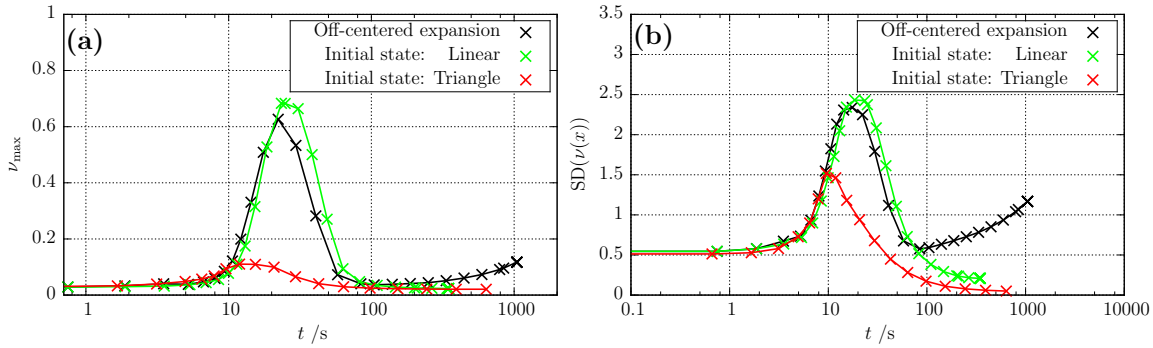

Figure 6.16: The evolution of $\nu_{\max}$ (a) and SD(ν) (b) for Fig. (6.13)-(6.15). In the homogeneous cases, the final values are lower than the initial ones.

7 Summary and discussion

The main result of this thesis is that it is possible to obtain homogeneous states from an initially inhomogeneous density distribution. The homogenization is due to dense, high-pressure regions, generated by the shaking procedure which expand after the shaking stops. These high-pressure regions arise through the vibrating walls, which accelerate the gas perpendicular to the wall towards the center. A necessary condition for an even expansion is the position of the barycenter during the expansion. This means, an all time centered barycenter leads to a homogenized state.

Another basic condition for this homogenization is the level of compaction during the shaking process. That is, too dense layers do not have the ability to expand in a way that leads to a homogenous state. The reason for this probably lies in the pair-correlation-function g_{Q} from Sec. (3.3). This includes the solid-liquid phase transition around $\nu_c \approx 0.7$ which causes a drastic change in slope of the pressure for this value of ν (see Fig. (3.1)). Because of that we throughout tried to avoid the occurrence of too compacted areas, with several vibration techniques such as the transient procedure, and a temporally limited vibration process which have delivered the desired results. In the case of an oscillation parallel to the density gradient (Sec. (6.2)) it is particularly simple to avoid these regions and to generate homogeneous systems, since the most compacted area is distributed in a symmetrical, centered stripe. The maximum packing fraction in Fig. (6.10) amounts merely to 0.11 for all examined frequencies and the system is far away from a phase transition. In comparison, the all-sided vibration generates compact areas in form of circles that tend to collapse during the shaking process and the maximum packing fraction is reached quite fast.

Another disadvantage of too compacted areas is the increased instability of the simulations. Because of this and other numerical issues, the explorable parameter space was limited to certain system sizes and packing fractions. A proposal to

stabilize the simulations is, to increase the resolution of the system. That is using higher resolutions such as 256^2 cells will smooth out the gradients of the physical fields. With an increased simulation stability, it would be possible to explore the stability of compacted areas more detailed. Thereby, in the all-sided shaking case, it could be possible to increase the total vibration time, which stabilizes the barycenter as in Fig. (6.10), without an abortion during the expansion. A low wall velocity $v_{\mathrm{w}} \propto fA$ may lead to a limited compaction of the high-pressure region (see Fig. (6.10)) and afterwards to an evenly expansion into a homogeneous state. Thus, a universal procedure is created, for which T_{tr}, T_E and T_{A} do not have to be tuned.

To actually be able to use theoretical predictions for experiments with granular gases one has to implement a more realistic wall-gas interaction. Walls without tangential friction may generate artificial states that are not observed in reality. Especially the states produced in Sec. (6.2) would not arise in the case of tangential friction. In addition, theoretical predictions in a 3D-system would be even more useful for experimentalists. However, it might be difficult to control the compacted areas because the hysteretic solid-liquid phase transition is even more apparent in 3D [7].

In conclusion, the all-sided shaking procedure is the single procedure to obtain a homogeneous state out of an arbitrary distributed initial state.

Bibliography

[1] N. Brilliantov and T. Pöschel, "Kinetic theory of granular gases", in (Oxford University Press, 2002) Chap. 1–23.

[2] T. Pöschel and S. Luding, "Granular gases", in (Springer, 2001) Chap. 2.

[3] M. Hummel, J.Clewett, and M. G. Mazza, under review (2015).

[4] K. Harth, U. Kornek, T. Trittel, U. Strachauer, S. Höme, K. Will, and R. Stannarius, Physical Review Letters **110**, 114102 (2013).

[5] V. Garzo and J. M. Montanero, Physica A **313**, 336 (2002).

[6] J. W. Dufty, J. Phys. Chem. C **111**, 15605 (2007).

[7] S. Luding, IOPscience **22**, R101 (2009).

[8] H. Versteeg and W. Malalasekera, "Computational fluid dynamics - the finite volume method", in (Pearson Education Limited, 2007) Chap. 1–13.

[9] J. Wang and G. Widhopf, Journal of Computational Physics **84**, 145 (1988).

[10] J. J. Brey, M. I. G. de Soria, P. Maynar, and V. Buzon, Physical Review E **88**, 062205 (2013).

[11] T. Barth and P. Frederickson, AIAA **90**, 26902 (1990).

[12] V. A. Titarev and E. Toro, Journal of Computational Physics **201**, 238 (2004).

[13] P. Müller, S. Antonyuk, J. Tomas, and S. Heinrich, "Investigations of the restitution coefficient of granules", in *Micro-macro-interaction*, edited by A. Bertram and J. Tomas (Springer Berlin Heidelberg, 2008), pp. 235–241.

[14] W. E. East, "Numerical hydrodynamics in strong-field general relativity", PhD thesis (University of Princeton, 2013).

[15] C. D. Muhlberger, "Numerical simulations of generally relativistic hydrodynamic systems", PhD thesis (University of Cornell, 2014).

Erklärung nach §18(8) der Prüfungsordnung für den Bachelor-Studiengang Physik und den Master-Studiengang Physik an der Universität Göttingen:

Hiermit erkläre ich, dass ich diese Abschlussarbeit selbständig verfasst habe, keine anderen als die angegebenen Quellen und Hilfsmittel benutzt habe und alle Stellen, die wörtlich oder sinngemäß aus veröffentlichten Schriften entnommen wurden, als solche kenntlich gemacht habe.
Darüberhinaus erkläre ich, dass diese Abschlussarbeit nicht, auch nicht auszugsweise, im Rahmen einer nichtbestandenen Prüfung an dieser oder einer anderen Hochschule eingereicht wurde.

Göttingen, den 15. Oktober 2015

(Marius Herr)